DOI: 10.1002/aenm.((please add manuscript number))
Article type: Review

Recent advances in conduction mechanisms, synthesis methods, and improvement strategies for $Li_{1+x}Al_xTi_{2-x}(PO_4)_3$ solid electrolyte for all-solid-state lithium batteries

Pengfei Wu, Weiwei Zhou, Xin Su,Jianyu Li, Min Su, Xiaochong Zhou, Brian Sheldon*, Wenquan Lu**

P. Wu, Prof. X. Su
Advanced Battery Technology Center, School of New Energy, Harbin Institute of Technology, Weihai, 264209, China
sux@hit.edu.cn

Prof. W. Zhou, J. Li
Advanced Battery Technology Center, School of Materials Science and Engineering, Harbin Institute of Technology, Weihai, 264209, China

Dr. M. Su, Dr. X. Zhou
R&D Center, Wanxiang A123 Systems Corp, Hangzhou, 311215, China

Prof. B.W. Sheldon
School of Engineering, Brown University, Providence, RI 02912, USA
Brian_Sheldon@brown.edu

Dr. W.Lu
Electrochemical Energy Storage, Chemical Sciences and Engineering Division, 9700 South Cass Avenue, Building 205, Argonne, IL 60439-4837, USA
wenquan.lu@anl.gov

Keywords: NASICON-type solid electrolytes; Lithium aluminum titanium phosphate; Lithium-ion conduction mechanisms; $Li_{1+x}Al_xTi_{2-x}(PO_4)_3$ synthesis; LATP improvement strategy

Abstract

With the increasing use of Li batteries for storage, their safety issues and energy densities are attracting considerable attention. Recently, replacing liquid organic electrolytes with solid-state electrolytes (SSE) was hailed as the key to developing safe and high-energy-density Li batteries. In particular, $Li_{1+x}Al_xTi_{2-x}(PO4)_3$ (LATP) has been identified as a very attractive SSE for Li batteries, due to its excellent electrochemical stability, low production costs, and good chemical compatibility. However, interfacial reactions with electrodes and poor thermal stability at high temperatures severely restrict the practical use of LATP in solid-state batteries (SSB). Herein, a systematic review of recent advances in LATP for SSBs is provided. This review starts with a brief introduction to the development history of LATP and then summarizes its structure, ion transport mechanism, and synthesis methods. Challenges (e.g., intrinsic brittleness, interfacial resistance, and compatibility) and corresponding solutions (ionic substitution, additives, protective layers, composite electrolytes, etc.) that are critical for practical applications are then discussed. Finally, an outlook on the future research direction of LATP-based SSB is provided.

1. Introduction

With the continuous development of electronic technology, a huge variety of electronic products—mobile phones, micro cameras, notebook computers, electric vehicles, and thousands more—have been created. Such enormous market demand has propelled the advance of batteries as the main power storage system.[1-8] However, conventional Li batteries often suffer from safety issues, including short circuits and even combustion. The former is due to Li dendrites puncturing the separator at high currents; the latter is caused by the oxidative decomposition of the organic liquid electrolyte (LE) at high temperatures, accompanied by the release of gas byproducts.[9-15] Solid-state battery (SSB) technology can avoid these issues by using a solid-state electrolyte (SSE), which has several significant advantages: Suppressing Li dendrites formation, which opens the door to utilize Li metal as the anode for high energy density. The replacement of separators and LEs with SSEs can significantly reduce the distance between the cathode and anode, which implies that SSB technology could potentially contribute to miniaturizing the batteries. SSB's (literal) flexibility should not be overlooked. By adopting appropriate encapsulation materials, an SSB can withstand bending without obvious degradation in performance.[16-20] Developing a high-performance SSB may represent a technological step forward in the battery field.

SSEs to date can be generally classified into three categories: polymers, sulfides, and oxides. Polymeric SSEs date back to an early report of the alkali ionic conductive behavior of polyethylene oxide (PEO) in 1973, since which time investigations of solid polymer Li batteries have become the focus of related research.[21-24] Compared to sulfides and oxides, polymeric SSEs are easy to process and integrate. However, polymer SSBs' low ionic conductivity and high thermal management requirements lead to large energy consumption and high cost.

Unlike polymeric SSEs, sulfides-based SSEs show ionic conductivity similar to that of conventional LEs. For example, the room temperature (RT) ionic conductivity of $Li_{10}GeP_2S_{12}$ (10^{-2} S cm^{-1}) is comparable to or even higher than that of LEs.[25-27] Moreover, sulfide-based

SSEs possess a wide electrochemical window and relatively good interfacial stability after the formation of solid electrolyte interphase (SEI) films. However, sulfides are chemically unstable in air and can produce toxic H_2S gas in the presence of water. [28,29]

In contrast to SSEs consisting of polymers and sulfides, oxides-based SSEs, sodium superionic conductor (NASICON) structured materials in general, can exhibit both good thermal/structural stability and high ionic conductivity, and they are becoming the hot materials for SSB.[30,31] In particular, $Li_{1+x}Al_xTi_{2-x}(PO_4)_3$ (LATP), as a typical NASICON-type oxide SSE, exhibits high ionic conductivity (10^{-4}~10^{-3} S cm^{-1}) and excellent stability in the presence of air and water.[32,33] Table 1 summarizes the basic properties of the common SSEs. It can be clearly seen that the LATP, as a typical oxides-based SSE, not only possesses superior conductivity to the polymer SSEs, but also has more stable electrochemical properties than the sulfides-based SSEs. Thus, it has attracted intensive research interests for SSB nowadays. Unfortunately, LATP has interface problems with Li metal: The high-valent metal ions Ti^{4+} are readily reduced at low potentials, leading to an increase in interfacial resistance or even rendering the SSB ineffective.[34,35]

The scientific and technical challenges facing LATP have generated great research interest.[36] However, the systematic evolution of LATP so far has not been well documented, nor have the dilemmas and solutions for the further development of a LATP SSE. Herein, the recent advances in the development of LATP SSE are systematically reviewed. In this review, we first introduce the research history of LATP SSE analytically, and summarize its structure, ion transport mechanism, and synthesis methods. The problems that LATP faces and their corresponding solutions are presented, and effective ways to reduce the impedance and improve the stability of the electrode/SSE interface are discussed (**Figure 1**). Finally, we outline the challenges and prospects involved in promoting the progress of LATP SSE in the future. Since there are few relevant reviews on LATP, it is hoped that the completion of this review will hopefully guide the future research and development of LATP SSE for SSB.

2. The Evolution of LATP

In 1976, a NASICON-type electrolyte was discovered in the framework of solid solution phase $Na_{1+x}Zr_2SiP_{3-x}O_{12}$.[37,38] Among NASICON-type electrolytes, Li-based NASICON-type electrolytes are considered most promising due to their good chemical stability and high ionic conductivity.[39] **Figure 2**a shows the structure of Li-based NASICON-type materials. It can be seen that Li is generally located at both M1 and M2 sites, and the hindrance to Li ion diffusion is a window between the M1 and M2 sites consisting of three O atoms bound to and adjacent M cation.[40] At present, there are four main types of NASICON-type electrolytes: $LiZr_2(PO_4)_3$ (LZP), $LiHf_2(PO_4)_3$ (LHP), $LiTi_2(PO_4)_3$ (LTP) and $LiGe_2(PO_4)_3$ (LGP). The progress of the ionic conductivity of these Li-based NASICON-type electrolytes is presented in Figure 2b. In the following, we describe the development of each $LiM_2(PO_4)_3$ (M=Zr, Hf, Ti, and Ge).

In 1986, Petit et al. first synthesized LZP with good electrochemical stability.[41] The ionic conductivity of LZP was only 5.0×10^{-6} S cm^{-1} at RT, and the Li ion diffusion activation energy was 0.43 eV.[42,43] After years of research, it was found that the conductivity of Li ions in LZP can be effectively improved by optimizing the amount and variety of doping elements and sintering conditions.[44-48] For example, the conductivity of internal Li ions in LZP can be efficiently raised by substituting Y^{3+} ions with Zr^{3+} and the assistance of spark plasma sintering (SPS).[45] However, LZP is susceptible to temperature and pressure. Its structure changes at different temperatures, especially at high temperatures.[49,50] This is possibly due to the closed Zr-O-P bond angle, which causes phase transitions and conformational changes in the coordination environment of Li.[51,52] Such an electrochemical instability of LZP is considered as a critical factor that hinders its practical applications.

Replacing Zr^{4+} with Hf^{4+} produces LHP, which has higher ionic conductivity since the "tunnel" is more suitable for the migration of Li ions. Especially at high temperature, the Li–O bond distance at the M1–M2 site in LHP increases, which can lead to a dramatic increase in Li mobility and thereby low activation energy.[53] It is well documented that ion substitution and

sintering process adjustments are good ways to improve the ionic conductivity of LHP-based electrolytes. Zangina et al. investigated the effect of Al substitution in LHP, and the results show that $Li_{1.25}Al_{0.25}Hf_{1.75}(PO_4)_3$ has a high Li ionic conductivity of 2.5×10^{-3} S cm^{-1} at RT.[54] Despite this, it should be noted that LHP undergoes a phase transition from rhombohedral to trigonal when the temperature is reduced to 0 °C. The strong delocalization of Li ions is detected at the M1 and M2 sites that severely limits the practical use of the LHP.[55,56]

Compared to other NASICON-type SSEs, LGP-based SSE remains electrochemically stable even at a high voltage window of 6 V. However, it has an ionic conductivity of only 10^{-7} S cm^{-1}.[25] To solve this problem, ion substitution and the addition of Li salts have proved effective.[57-60] Recently, $Li_{1+x}Al_xGe_{2-x}(PO_4)_3$ (LAGP) has attracted much attention due to its inherent high conductivity.[61-63] In addition, by doping LAGP with TiO_2, the bottleneck size of the Li^+ migration channel increases and the grain boundary area decreases, yielding the highest ionic conductivity: 1.07×10^{-3} S cm^{-1} at RT.[64] In addition to ion substitution, additives can also improve the performance of LAGP electrolytes.[65] However, the interfacial compatibility of LAGP with electrodes and the formation of Li dendrites still remain big problems, especially with severe side reactions with Li metal anodes.[66-71] Constructing composite electrolytes[68,69] and additive layers[66,67,70,71] are two directions in which the problems are being investigated. These two strategies can both prevent undesirable reactions between the Li and SEI and significantly reduce interfacial resistance and polarization. However, the higher price of Ge renders LAGP not very popular in the market.

Compared to LZP, LHP, and LGP, LTP was found to have the lowest activation energy, the highest ionic conductivity, and the most suitable lattice sizes for Li^+ migration.[72] In LTP, vacancy-assisted and interstitial Li ionic diffusions co-exist and work in tandem (Figure 2c). The activation energy for the diffusion of Li ions in the interstitial state is only 0.25 eV, which makes the interstitial diffusion easier than vacancy diffusion (0.42 eV).[73]

When LTP is used as an SSE, both the bulk conductivity and the total ionic conductivity must be taken into account.[74] However, the ionic conductivity of LTP is still not comparable to that of LEs. The use of additives[75,76] and element doping are effective ways to enhance the ionic conductivity of LTP. It has been shown that a partial replacement of Ti^{4+} and P^{5+} in LTP with M^{3+} (M^{3+} = Al^{3+}, B^{3+}, Cr^{3+}, Ga^{3+}, Fe^{3+}, Sc^{3+}, In^{3+}, Lu^{3+}, Y^{3+}, La^{3+}, Zr^{4+} and Si^{4+})[77-80] can perform well.[81] Of these, $Li_{1+x}Ti_{2-x}M_x(PO_4)_3$ (x=0.3, M=Al and Sc) can achieve the highest ionic conductivity (Figure 2d).[77,80] In particular, the Al^{3+} substitution that produces LATP has received significant interest and attention due to its low cost. Besides, the enhanced vibrations of O and P in LATP lead to local relaxation and changes in Li coordination, improving the conductivity of Li ions compared to LTP.[82] As research progressed, LATP, with excellent electrochemical stability and good conductivity, has become the mainstream study direction in the SSBs field. [77,83]

From 1980s to now, LATP has gone through a period of rapid development (Figure 2e). To be specific, in 1976, Goodenough et al. first designed the NASICON structure,[37,38] and then, as its important oxide SSE, LATP with high conductivity was reported by Aono et al. in 1989.[84] Later, the first oxide-based SSB consisting of $Li_4Ti_5O_{12}$/LATP/$LiMn_2O_4$ was built in 1999. The as-assembled cell delivered a small capacity loss after 10 cycles.[85] However, the LATP obtained via conventional annealing tended to form secondary phase $AlPO_4$ at 900 ℃. It was not until 2004 that the pure phase of LATP was synthesized.[86] In the subsequent years, numerous characterization technologies had been applied to study the ion transport mechanism in LATP. In 2017, He et al. discovered the co-migration mechanism of LATP, which greatly promoted the rational design of LATP.[87] In that period, the practical application of LATP was primarily hindered by the lack of rapid synthesis method since conventional sintering of SSE often needed several hours. Until just in 2020, Wang et al. has developed a ultrafast high-temperature sintering (UHS) process to realize the rapid synthesis of LATP within ~40 s.[88]

However, when LATP was integrated into SSBs, the as-fabricated SSBs only demonstrated modest electrochemical performance, in contrast to the intuitive and optimistic anticipations. The complicated interfacial challenges and its intrinsic brittleness are found to practically hinder the exploitation of SSBs capacity. To this end, strategies such as the addition of other solid or gel electrolyte to construct composite electrolytes have been proposed to improve the electrode−electrolyte interface and greatly progressed in the recent year.

In the above discussion, we briefly review the discovery process of LATP, focusing on the fundamental structure, Li ion conducting properties, and disadvantages of each $LiM_2(PO_4)_3$ (M=Zr, Hf, Ti, and Ge) phase. In the past years, abundant investigations have been devoted to developing practically accessible SSBs with LATP, during which much progress has been achieved. In the following discussions, we will focus on the conduction mechanism and synthesis methods of LATP, as well as the problems (high processing temperature, its intrinsic brittleness, and interfacial problems) it encounters and corresponding solutions (ionic substitution, additives, protective layers, composite electrolyte, etc.).

3. Microstructure and Conduction Mechanisms of LATP

LATP consists of TiO_6/AlO_6 octahedron and PO_4 tetrahedron, with the upper two TiO_6/AlO_6 octahedra and three PO_4 tetrahedra sharing oxygen atoms, forming the entire three-dimensional (3D) Li ion transport network (**Figure 3**a). Li is generally thought to have three distinct sites in the NASICON-type SSE. Figure 3b illustrates the distribution of M1 (Li1, 6b, sixfold oxygen coordination), M2 (Li2, 18e, tenfold oxygen coordination) and M3 (Li3, between M1 and M2, fourfold oxygen coordination) sites in the NASICON structure. These sites alternate along the Li^+ conduction pathway.[89] Generally, Li ions prefer to occupy the M1 sites in LTP , while in LATP they take possession of both M1 and M3 sites (Figure 3c).[90] Furthermore, researchers have found that substitution of Al^{3+} enhances the length of the Li-O bond, weakening the bond strength and thus increasing the rate of Li ion migration. As the Al

content increases, Li ions occupy more M3 sites and form less grain boundary resistance, which can thus improve the ionic conductivity of LATP.[90-92]

The 3D ion diffusion network within the LATP crystal skeleton endows LATP with excellent Li ionic conduction properties, and its superconductivity has led to a surge of research on the mechanism of Li ionic conduction in LATP. Rettenwander et al. proposed that the Li ionic conducting path in LATP follows the general NASICON structure type M1→M3→M1 in a co-migration approach.[93] Lu et al. investigated the conduction mechanism of Li ions and found that gap diffusion is more applicable to LTP. It can be seen from Figure 3d that in LATP, Li ions completely occupy the 6b sites, while the 36f sites near Al ions are partially occupied.[73] When LTP is doped with Al^{3+}, additional Li ions are introduced to balance the charge. The electrostatic force generated by these extra Li ions shifts the nearby Li ions from 6b to 36f sites, where split Li ions are formed at the 36f sites.[73,81,94,95] In LATP, the activation energies of these two sites are completely different, with a much lower activation energy at the 36f site than at the 6b site. The results suggest that the Al doping in LTP reduces the activation energy of nearby Li ions, and the disordered state of the Li ions site enhances the interstitial diffusion process of Li ions. This implies that the Li migration in LATP is driven by the interstitial diffusion between 36f sites.[93]

Pfalzgraf et al. analyzed the effect of LATP crystal structure on Li ion migration properties and concluded that the M2 transition state is stabilized due to the increased Al/Ti occupying the octahedral position near the M3 position, which leads to a lower migration potential barrier.[96] In Figure 3e, He et al. demonstrated the simultaneous occupation of the M1 and M2 sites by Li^+, and the strong interaction forces between them can effectively lower the diffusion potential barrier. This is crucial to activating the interstitial migration.[87] The potential barrier for interstitial migration is shown to be about 0.29 eV, which is significantly lower than the conventional value calculated for LATP migration (approximately 0.33 eV).[97] Clearly, the lower interstitial migration potential barrier contributes to the superconductivity of LATP.

In-depth study concerning the ion transport mechanism in LATP using advanced characterization techniques can help to establish the research basis for developing high-performance LATP. To date, numerous characterization technologies (such as X-ray tomography, X-ray spectroscopy, Raman spectroscopy, NMR and electron microscopy) have been applied to identify complex and elusive chemical/physical processes in SSBs. However, the ion transport mechanism in LATP has not been fully clarified yet, and this is a major obstacle to the practical design of LATP. Therefore, it is urgent to confirm the transport mechanism of Li ions in LATP and contribute to the rational design of LATP with the superconductive network. To this end, more emphasis should be put on studying the microstructure and conduction mechanisms of LATP, including the processes of LATP formation and conversion to final material, Li ion transportation pathways, as well as the detailed structure and composition of the LATP particles.

4. Synthesis Methods

To promote the use of LATP in SSBs, it is important to manufacture the materials with high Li^+ conductivity via a simple synthesis route. At present, the common methods for preparing LATP include melt quenching, mechanical activation, sol–gel, co-precipitation, hydrothermal, and so on. Here, our main focus is on the characteristics, basic processes and improvement strategies of these methods, although other recently emerged innovative methods have also been illustrated.

4.1 Melt Quenching Method

Melt quenching is the main commercial production route for high-density LATP. Waetzig et al. prepared LATP ceramics using the melt quenching method, achieving excellent densities (2.84 g cm^{-3}) between 900 ℃ and 1000 ℃.[98] Later researchers further treated the LATP glass-ceramics obtained by melt-quenching with microwave heating.[99] Compared to conventional heating methods, microwave heating allows for a higher heating rate, which significantly reduces the formation of secondary phases. **Figure 4**a shows the diffraction patterns of

conventionally heated and microwave heated samples at different temperatures. The conventionally heated product begins to form secondary phase $AlPO_4$ at 900 ℃, while in the microwave sample $AlPO_4$ only appears in the sample crystallized at 1000 ℃.

Obviously, temperature is an important factor governing the melt quenching method. Fu et al. further investigated the effect of temperature on the electrochemical properties of LATP. It was found that when the heat-treatment temperature was 950 ℃, the sample had high thermal resistance and could reach a maximum conductivity of 1.3×10^{-3} S cm^{-1} at RT (Figure 4b).[32] It should be noted that melt quenching usually requires a high reaction temperature (~1400 ℃) but with a low yield of the main phase. This may be due to the loss of Li_2O caused by evaporation, which leads to partial conversion of LATP into secondary phases, such as $AlPO_4$ at ~950 ℃.[98,100,101] As can be seen in Figure 4c, large grains and cracks appear in these secondary phases as the temperature increases, resulting in a decay of ionic conductivity.[98,102] Moreover, the high energy consumption caused by the high processing temperature (>1000 ℃) and the brittleness of the dense ceramic render the melt quenching method hard to be scaled up.

4.2 Mechanical Activation Method

As a solid-phase method that simplifies the preparation process, mechanical activation can directly reduce the particle size of the material and significantly lower the sintering temperature of the raw material.[103-105] It is well known that solid-phase methods usually require high temperatures and long reaction times to obtain the desired LATP.[106] In these cases, mechanical ball milling of the raw material, or mechanical activation, can reduce the particle size of the material, improve the interfacial stability of the electrolyte and also effectively reduce the temperature needed for the subsequent heat treatment. As a result, the phase homogeneity of the final product can be greatly improved.[105,107,108] It can be seen from **Figure 5**a that the particle sizes of the LATP powders obtained by mechanical milling for 40 h can be measured in 50 nm. Morimoto et al. found that the raw material can hardly be observed after 20 h of mechanical milling, which allowed for a complete reaction even at low heat-treatment

temperatures (Figure 5b).[109] He et al. used AlOOH as the Al source for the synthesis of LATP, which led to an easier substitution of Al^{3+} for Ti^{4+} in the LTP structure and resulted in a large number of Li vacancies and Li gaps. The conduction rate of Li^+ ions also increased.[110]

Due to the inevitable loss of Li during the reaction, the addition of excess Li in the initial material can effectively improve the ionic conductivity of LATP.[111] Xu et al. further modified the mechanical milling process for synthesizing LATP by adding an extra 10 wt% Li_2CO_3 to the precursor. This variation, exc-LATP, could not only compensate for the Li^+ loss during sintering but could also employ the excess Li_2CO_3 as a sintering additive. Moreover, ball milling results in good sintering activity and faster densification of the material, bringing the ultimate sintering temperature down to 775 ℃. Figure 5c shows that due to the smaller grain boundary thickness of exc-LATP compared to that of stoichiometric LATP (stoi-LATP), the limitation of the grain boundary on the Li ion transport is correspondingly reduced, and exc-LATP obtains a higher total ionic conductivity.[112]

4.3 Sol–Gel Method

The sol–gel method is a typical method for the preparation of glass ceramics, but unlike solid phase methods, it is capable of producing nanosized LATP particles at lower temperatures on a large scale. In addition, the electrochemical performance of LATP samples synthesized by the sol–gel method is superior to those obtained from the solid phase method.[86,113,114] However, LATP materials synthesized by the sol–gel method tend to form agglomerates and have a low density. This can be avoided by the addition of dispersants.[115] For example, Zhao et al. synthesized LATP using ethylene glycol or glucose as a dispersant, and they found that the LATP sample obtained with glucose as a dispersant was less agglomerated and had improved electrochemical properties compared to its counterparts with ethylene glycol. This is because the hydroxyl groups of glucose bridged the metal complexes and prevented them from contacting with each other through a spatial site barrier effect.[106]

In the development of a sol–gel method for LATP, researchers have made many advances in improving the choice of precursor, the optimization of the reaction catalysis, and the use of solvents for precursor dissolution.[100,116-118] Liu et al. developed a two-step heat treatment, annealing the dry gel in argon and air successively (**Figure 6**a). Such a two-step treatment can protect the LATP particles from aggregation while yielding a narrower particle size distribution.[116] Kotobuki and Koishi investigated the electrochemical properties of LATP prepared by the sol–gel method with different Al sources. It is found the $Al(NO_3)_3$ source introduces an impurity phase $AlPO_4$ into the final LATP product due to its insufficient mixing with other raw materials. This would cause adverse impact on the ionic conductivity of LATP since such an impurity phase can act as a resistive layer (Figure 6b). While in the case of employing $Al(C_3H_7O)_3$ as Al source, the $AlPO_4$ formation is not observed. Thus, the LATP obtained from $Al(C_3H_7O)_3$ exhibits higher Li ion conductivity than the counterpart obtained from $Al(NO_3)_3$.[119]

4.4 Co-Precipitation Method

The co-precipitation method has the advantages of low synthesis temperature and short sintering time, which make it possible to reduce the processing costs of LATP. This makes it a suitable method for large-scale production. Kotobuki and Koishi prepared LATP by co-precipitation and investigated the effect of calcination temperature on the properties of the resulting LATP samples.[120] **Figure 7**a shows that LATP prepared at 800 ℃ was completely crystallized, and the sample sintered at 1000 ℃ displayed excellent ionic conductivity. Adding a sintering aid can further reduce the sintering temperature. Odenwald et al. used Li_2WO_4 as a sintering aid for LATP electrolytes. Figure 7b shows that pure LATP shows only a small amount of densification below 950 ℃. In contrast, the addition of Li_2WO_4 not only significantly reduces the sintering temperature but also increases the densification of LATP.[121] Designing a rational sintering process can modulate the conductivity of LATP as well.[122] For example,

Duluard et al. combined a co-precipitation method with an SPS technique. Compared to conventional sintering, SPS can provide a faster ramp rate and thereby reduce the formation of secondary phases during the sintering process, producing LATP with excellent ionic conductivity.[123]

4.5 Hydrothermal Synthesis Method

The hydrothermal method is another wet-chemical way to precisely control the composition and morphology of the prepared materials, and it is able to produce LATP precursors in a lower temperature range. It should be noted that synthesis conditions have a strong influence on the electrochemical performance of hydrothermally produced LATP.[124] For example, after exploring a series of parameters, Kim et al. found that the optimum hydrothermal reaction time for the synthesis of LATP was 12 h, and the calcination and sintering temperatures were 600 ℃ and 900 ℃, respectively (**Figure 8**a).[125] Peng et al. carried out a further study on the hydrothermal method based on additional amounts of Al sources. All LATP samples show three peaks (Li1 and Li2, which are two upper field narrow peaks, and Li3, a broad lower electric field peak) except for sample LATP-$_{Al/Ti-0.2}$. In general, the lower electric field broad peak Li3 has a lower ion mobility, while the Li ions occupying the Li1or Li2 positions show a narrower line, indicating a fast mobility of Li ions. The Li1 and Li2 peaks of the LATP-$_{Al\ /Ti-0.2}$ sample are aligned into a single peak, indicating that the Li ions at the M1 position are excited to high-mobility Li ions, resulting in an increase in the ionic conductivity of the LATP-$_{Al/Ti-0.2}$.[126] With the optimization of the sintering process, the electrochemical properties of LATP by hydrothermal synthesis have also been greatly improved.[127] Hallopeau et al. used microwave-assisted reactive sintering for the hydrothermally yielded LATP precursor. Figure 8b shows that the increase in activation energy at higher temperatures indicates a change in the conduction path of Li ions. Compared to conventional sintering methods, microwave sintering reduced the formation of secondary phases due to less sintering time, which significantly improved the ionic conductivity of the products.[128] Recently, He et

al. used a hydrothermal method to synthesize a unique rhombic phase LATP (Figure 8c). The result shows that the LATP sample exhibited a uniform particle size distribution and less agglomeration.[129]

4.6 Other Methods

In addition to the relatively common methods above, recently some new ways to prepare LATP, like spray drying,[130,131] the template method,[132] direct ink writing (DIW),[133] and large-area pulsed laser deposition (PLD),[134] etc. have emerged. For example, Liu et al. successfully synthesized LATP using the DIW method (**Figure 9**a). The prepared ink has suitable rheological properties and can be extruded into different shapes. Moreover, DIW can even print the electrolyte directly on the cathode of the SSB, effectively solving the interface problem between the LATP SSE and the cathode.[133] Siller et al. used PLD to synthesize LATP nanoparticles deposited uniformly in the ground state, enhancing the density of LATP (Figure 9b, c).[134]

Conventional sintering of SSE often requires several hours, which may cause severe volatility of Li and further impede its application in large-scale production of SSBs.[91,135-138] Therefore, innovative sintering techniques with much-reduced sintering time, such as microwave-assisted sintering,[128] SPS,[123] flash sintering,[139] cold sintering,[135,140] field-assisted sintering technology (FAST),[141] ultrafast high-temperature sintering (UHS),[88] and others have been investigated. Wang et al. developed an UHS process in which the precursor reacted and densified rapidly, in about 40 s (less than 30 s of temperature rise and about 10 s of isothermal sintering), and the product exhibited a relatively small grain size (Figure 9d). Such a rapid reaction process can effectively reduce the formation of secondary phases, yielding a product with desirable properties.[88]

Despite the high efficiency, processing costs should not be ignored for these methods. Cold sintering's low sintering temperature and impurity-free product represents a new direction

for the preparation of SSE at low cost (Figure 9e).[140] **Table 2** summarizes some parameters of the synthesis methods above and the properties of their LATP products.

Overall, the major synthesis routes for LATP electrolytes can be classified into solid-state reactions (melt-quenching and mechanical activation) and wet chemical processes (sol–gel, co-precipitation, and hydrothermal). It is easy to discover that conventional solid-state reactions such as melt-quenching and mechanical activation not only require long fabrication time and high temperature but also lead to the LATP products with impurity, brittleness, and inhomogeneity. In contrast, liquid-phase synthesis routes for LATP (sol–gel, co-precipitation and hydrothermal) have been demonstrated to be more suitable for mass production by virtue of their low synthesis temperature, short reaction time, high controllabilty, and applicability for composites synthesis. Nevertheless, there are still some concerns to be addressed. For example, the wet reaction routes often involve unclear reaction mechanism, which can lead to unknown impurities. In addition, wet chemical routes are usually accompanied by the poor ionic conductivity of the products. Last but not least, the toxicity of the organic solvents used in some liquid phase processes should also be taken into consideration. Therefore, it is highly desirable to develop a facile, low-cost, and scalable synthesis route towards mass production of high-quality LATP.

5. Problems and Improvement Strategies

Although LATP has received a lot of attention by virtue of its excellent ionic properties and electrochemical stability in the NASICON-type family, it still has some problems. In this section, we present the challenges (e.g., low ionic conductivity, interface problems with electrodes, poor thermal stability) faced by LATP SSEs at this stage and corresponding improvement strategies (ionic substitution, additives, protective layers, co-sintering, etc.).

5.1 Improved Strategies for Increasing Ionic Conductivity

The ionic conductivity of LATP can be improved mainly by increasing the concentration of Li^+ ions in each cell or enhancing the mobility of Li^+ ions.[20, 56] The specific methods (ionic

substitution and additives) to increase the ionic conductivity of LATP SSE are described in detail below.

5.1.1 Ionic Substitution

In LATP, the most important contribution of Al^{3+} doping to ionic conductivity is to increase the Li ionic concentration.[48] Ionic substitution changes the lattice constants of the LATP crystal structure and the bottleneck size for Li ion migration. As a result, both the room for Li ion diffusion and the concentration of mobile Li ions increase, thus effectively improving the ionic conductivity.[107,142] Chang et al. performed a partial substitution of P by V ions in LATP, resulting in an increase in the mobile Li content and a decrease in the grain boundary resistance. Consequently, the barrier for Li migration at the grain boundary was reduced, enhancing the ionic conductivity.[91] Zhao et al. prepared a series of $Li_{1.3}Al_{0.3-x}Y_xTi_{1.7}(PO_4)_3$ electrolytes.[143] The results showed that Y substitution stabilized the electrolyte structure at lower sintering temperatures, and the YPO_4 phase in the doped electrolyte can be separated to grain boundaries, promoting effective densification of the electrolyte.[144,145] Note that the high density of the electrolyte can reduce the grain boundary resistance, which contributes to the high conductivity of the Li ion. Liu et al. doped LATP with the non-metallic element Si, which not only improved the thermal stability of the electrolyte but also changed the bottleneck size for Li ion migration. The substitution of Si facilitates the movement of Li ions, resulting in $Li_{1.7}Al_{0.3}Ti_{1.7}Si_{0.4}P_{2.6}O_{12}$ (LATSP) with excellent ionic conductivity up to 1.33×10^{-3} S cm^{-1} at RT.[146] In addition to these cationic substitutions, anionic substitution is also an effective means to improve the ionic conductivity of LATP. For example, Li et al. synthesized different levels of Cl-doped LATP, in which Cl atoms are randomly replaced by O atoms, the Li-O bonds at some positions are extended, and the change in the Li ion coordination environment improves the Li ion transport within the grain boundaries. These led to a significant enhancement of the ionic conductivity of pristine LATP.[147] Kızılaslan et al. synthesized S-doped LATP, which can provide more room for ion diffusion because replacing O with large-radius S would expand

the lattice. Moreover, Li ions can move more freely in S-doped LATP, since a weaker coulombic force is generated between S and Li ions because the electronegativity of S is smaller than that of O, thus increasing the ionic conductivity of the product.[148] **Table 3** summarizes recent advances in various types of ionic substitutions in LATP.

5.1.2 Additives

In addition to ionic substitution, additives work well to improve the ionic conductivity of the electrolytes. In general, adding some other phases to LATP can lower the sintering temperature and increase its density to bring down the grain boundary resistance, thus improving its ionic conductivity.[149,150] For example, Kwatek et al. chose $Li_{2.9}B_{0.9}S_{0.1}O_{3.1}$ glass (LBSO) as an additive to improve the ionic properties of LATP. During the sintering process, the LBSO glass transforms into a liquid phase. This can effectively cover the grains, fill the pores and promote the densification process of LATP to further increase its ionic conductivity.[74] Yang et al. reported the preparation of LATP membranes using PEO as a binder and borated polyethylene glycol (BPEG) as an additive. The addition of BPEG can not only enhance ionic conductivity by destroying the crystallinity of PEO, it fills the gaps between the particles with the assistance of PEO to provide more Li ion transfer pathways (**Figure 10**).[151] Kang et al. synthesized a series of LATP with SnO-P_2O_5-MgO (SPM) glass additives. The addition of SPM changed the distance between the Al/Ti-O and P-O bonds and further caused a gradual contraction of octahedral AlO_6 and tetrahedral PO_4, thereby increasing the ionic conductivity and the densification of LATP.[152] Researchers have also used Nb_2O_5[153] or B_2O_3[154] doping to precipitate unwanted phases during heat-treatment and effectively increase the ionic conductivity of LATP.

The mechanical properties of LATP can also be improved by adding another phase. Athansiou et al. demonstrated this with reduced graphene oxide (rGO), where the fracture toughness was more than doubled by adding only 1% rGO. And due to the experimental

selection of suitable process parameters, the ionic conductivity of LATP was also improved.[155] **Table 4** summarizes recent advances in various types of Additives in LATP.

5.2 Improvement Strategies for the Interface Between SSE and Electrodes

In addition to low ionic conductivity, LATP's chemical/electrochemical incompatibility with electrodes and thermal stability are essentially fatal issues. In this section, we present the causes of interface problems between LATP and electrodes and corresponding strategies (surface modification, co-sintering, etc.) to solve them.

5.2.1 Cathode Interface Improvement Measures

In the case of LATP contact with the cathode (**Figure 11**a), the difference in Li concentration (i.e., higher Li concentration in the cathode) leads to a transfer of Li to LATP. With electrons remaining on the cathode side, an electrical double layer (EDL) forms at the interface of the LATP SSE and cathode.[156] The transfer of Li ions to LATP and the retention of electrons in $LiCoO_2$ (LCO) may be responsible for the reduction in LCO content. In addition, the removal of oxygen and the driving force of charge neutrality during annealing, as well as the lower Li vacancy formation energy near the interface after charging, leads to the dynamic depletion of Li ions at the LATP/LCO interface. Figure 11b shows the deterioration of different cathode-to-LATP interfaces and the formation of a second phase at high temperatures. The degradation of the cathode phase will occur at relatively low temperatures (600 ℃–700 ℃) due to the diffusion of Li.[157] Therefore, it is necessary to develop more effective strategies (introduction of protection interlayer, co-sintering, etc.) to further optimize the interface between LATP and cathode.

Protection Interlayer

In recent years, introducing a protective layer between the cathode and SSE to restrict anion migration and reduce space charge accumulation has been found to effectively address the interface problems at the cathode.[158] For instance, Jin et al. used polymethyl methacrylate (PMMA) as an interfacial coating and constructed an interconnected 3D LATP framework

through intermolecular interactions between PVDF and PMMA (**Figure 12**a). The inherent Li ion complexation capability of PMMA ensured continuous Li ionic conduction through the LATP backbone and interface. The NCM/LATP@PMMA-PVDF/Li SSB displayed an excellent initial discharge capacity of 131.8 mAh g^{-1} at 0.5 C, with a capacity retention of 91.2% after 150 cycles.[159] Liang et al. coated an oxidation-resistant polyacrylonitrile (PAN) based polymer electrolyte film on the cathode side $LiNi_{0.6}Mn_{0.2}Co_{0.2}O_2$ (NCM622) of the LATP ceramic sheet (Figure 12b). Compared to the full cell without PAN coating, anions were greatly restrained and evenly distributed across the interface, stabilizing the interface by inhibiting anion migration and side reactions. The Li/LATP/NCM622 full cell had an initial discharge capacity of 168.2 mAh g^{-1} at 60 ℃ and 0.1 C, with a capacity retention of 89% at 0.5 C after 120 cycles.[160] Yang et al. used PEO instead of PVDF as an interfacial binder to prevent contact reactions between the electrode and SSE. Figure 12c shows that PEO can perfectly fill the gap between the cathode and LATP and greatly reduce the interfacial resistance. The Li/LATP/$LiFePO_4$ (LFP) SSB with PEO adhesion exhibits excellent reversible capacity and stable cycling performance at a current of 0.3 C.[161] Yu et al. coated a polymer film consisting of high Li^+ conductive polyphosphonitrile and mechanically stable PVDF-co-hexafluoropropylene on the cathode. The introduction of a polymer film increases the contact area between the electrode and electrolyte, enabling the LATP ceramic to work in a wide window and stabilizing the interface. The prepared SSB exhibited high mechanical, chemical and electrochemical stability with negligible capacity loss over 500 cycles at 50 ℃ (Figure 12d).[162]

Co-Sintering

The co-sintering of electrodes and SSE has no significant new phase formation, and the resulting interface is electrochemically active, which can effectively solve the interfacial contact problems.[163-165] Nanno and Nagata co-sintered the active materials $LiCoPO_4$ and

$Li_3Fe_2(PO_4)_3$ with LATP SSE. **Figure 13**a,c show that no other secondary phases were formed after the heat treatment, demonstrating that co-sintering can constrain the side reactions at the interface between the electrode and SSE, effectively improving their interfacial contact.[166] A suitable sintering temperature turns out to be a key factor in the improvement of interfacial contact. Kato et al. co-sintered the cathode material $LiNi_{1/3}Co_{1/3}Mn_{1/3}O_2$ (NMC) with LATP SSE and investigated the interfacial structure of NMC/LATP sheets at different sintering temperatures (700 °C–900 °C). As can be seen in Figure 13b,d, compared to the NMC-700/LATP interface, a reduced Co^{2+}-rich region exists around the NMC-900/LATP interface. Thus Co^{2+} diffuses and accumulates towards LATP to form a Li-free crystalline phase, resulting in an interfacial impedance (179 kΩ) that is three orders of magnitude larger than that of NMC-700/LATP.[167]

5.2.2 Li Metal Anode Interface Modulation Strategies

The interfacial issues between LATP and the anode need urgent attention. The high impedance and surface instability of LATP with Li metal retard its practical application. This mainly reflects in the following two aspects: (1) LATP has a high interfacial resistance with the Li anode. LATP is considered to be unstable to Li metal since it has a reduction potential as high as 2.16 V *vs.* Li.[156] The electrons obtained by LATP from the Li anode leads to a partial reduction of Ti^{4+} to Ti^{3+} on the LATP side (**Figure 14**a), which results in a higher electronic conductivity at the interphase. This would enable the rapid electron transport through the interface to the electrolyte, thus leading to the constant consumption of the electrolyte.[168] Moreover, the reduction of Ti^{4+} also leads to the presence of interfacial phases, which brings about mechanical instability of LATP. The ion transport is hindered once mechanical cracks are formed.[169] (2) The unstable Li/LATP interface leads to severe side reactions between them. Undesirable Li dendrites tend to nucleate and grow in the SEI at the Li/LATP interface. The growth of such highly reactive Li dendrites will react with the electrolyte, which in turn further accelerates the side reactions.[170] In conclusion, the chemical, electrochemical, and mechanical

incompatibilities of LATP with Li result in limited electrochemical window, increased grain boundary resistance, and growing cracks at the Li/LATP interface.

In the following sections, we present potential solutions to the issues concerning the interface between the Li anode and LATP.

Organic Polymer Coating

The use of an organic polymer coating would be a good way to solve the above interfacial problems (reduction of Ti^{4+}, grow of Li dendrites, mechanical instability). Such a polymer coating can prevent direct contact between LATP and Li metal and not only act as an artificial SEI to achieve rapid and homogeneous Li ion transport, but inhibit the continuous deterioration of LATP. What's more, this protective layer effectively prevents the interfacial reaction between Li and LATP by inhibiting interfacial electron transfer, thus maintaining stability after repeated cycles (Figure 14b).[171] Jin et al. introduced a composite polymer electrolyte (CPE) at the LATP/Li interface (Figure 14c), which can avoid side reactions between LATP and Li by inhibiting the formation and penetration of Li dendrites while ensuring effective Li ion transport. The overpotential of the symmetrical Li battery is significantly reduced, and the interfacial resistance decreased from 2852 to 505 Ω cm^2, allowing stable cycling for over 400 h.[172] Tang et al. used LE drops on the LATP/electrode interface and found that the addition of LE formed a stable solid–liquid electrolyte interface at the LATP/Li interface, thus hindering the reaction between them. The LFP/LATP-15% LE/Li SSB delivered an excellent initial discharge capacity of 151 mAh g^{-1} at 0.1 C, with a capacity retention of 96.5% after 100 cycles.[173]

However, LE is thought to gradually deplete due to its reaction with the anode Li, leading to the deterioration of the interfacial contact and eventual cell failure.[174] Therefore, Cao et al. coated the anode surface with a liquid-free plastic composite interlayer (PCI) consisting of amber nitrile and PAN, which localizes electrons and prevents their transfer from the anode to the SSE. In addition, it can reduce the voids caused by rigid surfaces and achieve close contact between LATP and Li metal, thus effectively reducing the interfacial impedance. Figure 14d

shows that PCI symmetric cells exhibited long cycle times, and the LFP/PCI/LATP/PCI/Li cells maintained 87.9% of their discharge capacity after 170 cycles at 0.1 C.[175] Chen et al. coated an ultrathin poly [2,3-bis(2,2,6,6-tetramethylpiperidine-N-oxycarbonyl)-norbornene] (PTNB) polymer on the anode Li. The PTNB protective layer has a fast self-exchange reaction of nitrogen-oxygen radicals, which promotes the transport of Li ions and thus inhibits the formation of Li dendrites. Figure 14e shows that the SSB with PTNB displayed a much higher initial capacity (158.7 mAh g^{-1}) than the cell without PTNB protection.[176]

Inorganic Coating

The polymeric film protection layer described above generally requires a complex preparation process, so an inorganic oxide layer with a relatively simple synthesis procedure would be more desirable.[177] He et al. coated the surface of LATP particles with a ZnO layer using magnetron sputtering (**Figure 15**a-c). The resulting sample displays reduced interfacial impedance (from 80554 to 353 Ω), which can be attributed to the formation of Li_2O in the presence of the ZnO layer, which can accelerate the transport of Li^+. Moreover, the side reactions and Li dendrites are effectively prevented by the inhibited transport of electrons in Li and LATP and the formation of unstable mixed conducting interphases, respectively. As a result, the LFP/ZnO@LATP/Li SSB had an excellent initial discharge capacity of 167.3 mAh g^{-1} at 0.1 C, with a capacity retention of 88% after 200 cycles.[178] Liu et al. deposited a nanosized Al_2O_3 layer on the LATP surface , aiming to stabilize the LATP/Li interface by reducing side reactions. Figure 15d shows the excellent cycling behavior of the LATP electrolyte coated with Al_2O_3 (LATP@150Al_2O_3), revealing a large overpotential of 10 V obtained in the first cycle. More important, the overpotential remained stable even after 300 cycles (600 h).[35]

Yang et al. coated the Li metal surface with a nanocomposite protective layer consisting of MgF_2, LiF and B_2O_3. As can be seen from Figure 15e, the resistance and interfacial impedance of the LATP with the composite coating do not increase as much as those of the uncoated counterpart, indicating that the protective layer effectively prevented the interfacial

reaction between the coated Li and LATP. The LFP/LATP/Li-coated SSB also exhibited good cycling performance and high reversibility (Figure 15f).[179]

5.2.3 Thermal Stability Improvement Measures

As is well known, Li metal is highly reactive and can generate a large amount of heat during battery failure.[180] High temperatures can also cause Li intrusion, and its reaction with SE at the defect further leads to a significant reduction in thermal stability.[168] Consequently, the thermal stability of the Li/LATP pellets is compromised, and the oxygen released by the SE at high temperatures triggers a highly exothermic reaction with the molten metal Li (**Figure 16**a,b), leading to thermal runaway.[181] Therefore, improving the thermal stability of Li metal is imperative for the use of LATP.

Recently, researchers have mainly employed surface modification and sintering additives to improve the thermal stability of the interface.[182,183] For example, Yu et al. added $LiPO_2F_2$ to modify the defective sites of LATP particles. As a result, direct contact between the LATP defect sites and Li can be avoided, thus significantly delaying thermal runaway (Figure 16c).[168] Xia et al. coated the LATP with an organic/inorganic composite layer of boron nitride-based release agent (BNRA). In addition to improving the interfacial contact between LATP and the electrode, BNRA also ensures timely thermal diffusion in the cell by virtue of its good thermal stability. Figure 16d shows the temperature curve of LATP and BNRA-LATP samples. It is clear that the BNRA-LATP displays faster thermal dispersion than bare LATP after the same thermal radiation, confirming that BNRA contributes greatly to the thermal stability of LATP.[184]

5.3 Strategies for Constructing Composite Electrolyte

On the one hand, LATP has attracted tremendous attention owing to its high ionic conductivity and excellent electrochemical stability. Nevertheless, in order to achieve dense ceramics with high ionic conductivities, high sintering temperatures of >1000 ℃ are usually required. The high processing temperature, its intrinsic brittleness, and the

chemical/electrochemical incompatibility between LATP and electrodes pose critical limitations for its practical applications.[185] On the other hand, solid polymer electrolytes (SPEs) are favored by researchers because of their satisfactory mechanical flexibility, improved interfacial contact and the compatibility with roll-to-roll manufacturing processes. However, their applications are limited due to their poor conductivity, narrow electrochemical window and suboptimal mechanical property.[186,187] Consequently, by the combining the merits of LATP and SPEs, the flexibility, mechanical property and conductivity of composite electrolytes can be enhanced to a great extent.[188]

5.3.1 Solid composite electrolyte

Conventionally, the design of on composite electrolytes has employed the dispersion of ceramic fillers into polymers. The size and concentration of fillers as well as the interface and structural design between fillers and polymer matrices, will both determine the percolated network of ionic conduction. To enhance the conductivity, the optimal fillers loading in composite electrolytes is generally between 10 and 15 vol%, where discrete ceramic particles are dispersed homogenously in the polymer matrix.[189,190] Increasing the concentration of fillers can immobilize Li salt anions through Lewis acid-base interaction to construct a percolated network, which will increase the ionic conductivity effectively. However, the filler particles tend to agglomerate once the increase of particle proportion in composite electrolytes exceeds the ceramic percolation threshold. Therefore, the structural design of the filler/polymer interface is crucial to prevent the agglomeration effect at high fillers concentration.[191] Meanwhile, the traditional fabrication of composite electrolytes with discrete particles is also difficult to take full advantage of the high ionic conductivities of the ceramic components. With this concern, the synthesis of solid composite electrolytes to break the aforementioned threshold of solid electrolytes has become a hot research topic.

PEO-based Composite Electrolyte

The interfacial degradation of Li/LATP is considered as a serious limitation for the practical application of LATP. When incorporating with SPEs, the LATP filler particles are well wrapped in SPEs chains, and the reaction between the LATP and Li metal anode is effectively prevented, therefore the interfical degradation can be minimized.[192] As a typical demonstration, Manthiram and Yu incorporated LATP nanoparticles with a PEO-$LiCF_3SO_3$ matrix. The composite PEO-$LiCF_3SO_3$-LATP SSE showed a reasonable ionic conductivity of 1.6×10^{-4} S cm^{-1} at 60 ℃, with reduced interfacial problems, and brittleness features. As a result, the LFP/ PEO-$LiCF_3SO_3$-LATP /Li SSB exhibited an excellent initial discharge capacity of 118.2 mAh g^{-1} at 0.5 C, with a capacity retention of 99% after 1000 cycles.[193] (**Figure 17**a) To enhance the ionic conductivity, one effective approach is to optimize the structural design of the filler/polymer interface (vertically aligned ceramic framework with the lowest tortuosity) which can provide continuous ion-conducting pathways.[194] Fan et al. designed a 3D interconnected porous LATP framework using NaCl as the template (Figure 17b). The 3D LATP framework could provide long-range and continuous percolation network and sufficient mechanical modulus, therefore promoting Li^+ fast transmission and preventing the growth of Li dendrites. As a result, the LFP/ 3D LATP composite electrolyte /Li SSB had an excellent long-term stability at 1 C.[195]

However, the above SSE , like most composite electrolytes, does not have sufficiently high ionic conductivity at RT for practical applications. In this regard, Li et al. introduced a conventional fluoroethylene carbonate (FEC) additive into composite electrolytes consisting of PEO matrix and LATP fillers, (Figure 17c) FEC-derived species were generated from the interaction between FEC and LATP, and thus resulted in an improved high ionic conductivity of 1.99×10^{-4} S cm^{-1} at 30 ℃.[196]

PVDF-based Composite Electrolyte

In addition to the PEO-based composite electrolyte mentioned above, the PVDF-based electrolytes also attracted much attention for their merits of high mechanical strength and excellent thermal stability. However, they have been faced with many serious issues due to the existence of N-dimethylformamide (DMF) residual solvent (DMF reduces the compatibility of PVDF-based electrolytes with high-voltage cathodes and Li metal anode).[197,198] Therefore, it is quite significant and critical to develop an innovative strategy to reduce the impact of the residual DMF in PVDF-based electrolytes. LATP with high ionic conductivity and excellent chemical stability is considered to tightly immobilize the DMF solvent and thus suppress the side reactions.[199] Zhong et al. incorporated LATP nanowires with a PVDF matrix. The LATP nanowires together with the PVDF polymer matrix created multiple and synergistic Li transport channels (Figure 17d), which greatly enhanced the ion transport efficiency.[200]

Clearly, the LATP fillers would immobilize anions via Lewis acid-base interaction, thus enriching the Li^+ at the LATP/polymer interphase.[201] Nevertheless, the discrete LATP ceramic fillers are dispersed randomly in polymer electrolyte prone to agglomerate after passing the percolation threshold.[202] Xiong et al. constructed a 3D Si@LATP/PVDF composite fiber network as an ion-regulative skeleton, by dispersing silane-modified LATP into a PVDF matrix. On the one hand, the 3D interpenetrating fibrous network can form more continuous Li^+ conduction pathways to improve the Li^+ ionic conductivity. On the other hand, The Si@LATP fully exposes the Lewis-acid sites of LATP and further enhances the anion adsorption ability. As a result, the LFP/ Si@LATP/PVDF /Li SSB exhibited an excellent initial discharge capacity of 150 mAh g^{-1} at 0.5 C, with a capacity retention of 99% after 200 cycles (Figure 17e).[203]

5.3.2 Gel Composite Electrolyte

The interfacial contact can be improved via the incorporation with SPEs, which are more flexible and highly compatible with electrode materials.[204] However, a significant downside

of this strategy is that tge differences in Li transport channels between electrolyte layers can result in the formation of a high interfacial energy barrier across the battery.[205] As a result, another strategy that has been used to improve the interfacial interactions in LATP-based SSB is to mix LATP with a small amount of ionogel electrolyte (negligible vapor pressures, robust ionic conductivity, thermal stabilities, and wide electrochemical window) for the purpose of modifying the unsatisfactory interfacial contact properties.[206-208]

A typical example was demonstrated by Zhang et al., who prepared a novel "Ionogel-in-Ceramic" composite electrolyte, by combining LATP ceramic particles with "PolyILs-in-Salt" ionogel, via a grinding and pressing method. (Figure 17f) The "PolyIL-in-Salt" with co-coordination not only can uniformly redistribute Li^+ in the gel composite electrolyte which can effectively provide efficient Li^+ conducting pathways, but also buffers the volumetric change of the SSE. The LFP/ LATP/ PolyIL-in-Salt /Li SSB had an excellent initial discharge capacity of 160 mAh g^{-1} at 0.1 C, with a capacity retention of 99.6% after 100 cycles.[209]

6. Summary and Perspectives

NASICON-type SSEs have attracted much attention due to their inexpensive raw materials, high ionic conductivity, and superior electrochemical properties. These advantage prompted us to systematically review recent advances of LATP SSE materials. In this effort, we reviewed the evolution of LATP, beginning with NASICON-type Na-based electrolytes, and summarized the diffusion mechanism of Li ion in LATP. Researchers have found that Al substitution not only enhances the density of LATP but also increases the concentration of Li ions, leading to a lower potential migration barrier. We also summarized synthesis methods that have been employed for LATP, including melt quenching, mechanical activation, sol–gel, co-precipitation and hydrothermal synthesis, with their respective advantages and disadvantages. Finally, the causes of and solutions for interfacial problems between LATP and electrode materials were described and illustrated.

NASICON-type SSEs have made significant progress in terms of ionic conductivity, electrochemical stability, mechanical stability, and interfacial contact problems. There are still many issues to be addressed: (1) The Li ionic conduction mechanism of LATP SSE should be better understood with the help of advanced characterization tools. (2) Although there is now a variety of methods to synthesize LATP, the large-scale preparation of LATP has not yet been achieved. This directly impacts the practical application of LATP SSE and the development of SSBs. (3) The causes of battery performance degradation after long cycle operation of an SSB have not been systematically investigated, and such work would be beneficial for speeding up the industrial implementation of SSB. (4) The high processing temperature, intrinsic brittleness, and the interfacial contact problems of LATP still remain unresolved and greatly restrict its practical applications. Despite these, the potential of using LATP with other electrolytes to construct composite electrolytes should not be ignored. (5) At present, there is still a lack of systematic research on the thermal stability of SSB, and safety issues could potentially threaten the commercialization of SSBs. We believe that long-term development of LATP can potentially enhance the competitiveness of SSB in the future.

Acknowledgements

P. W. and W. Z. contributed equally to this review article. X. S. would like to thank the support of the Young Taishan Scholars Program of Shandong Province and National Science Foundation from Shandong Province (2022HWYQ-074).W. L. gratefully acknowledges the support from the U.S. Department of Energy's (DOE) office of Energy Efficiency & Renewable Energy (EERE) Vehicle Technologies Office. Argonne National Laboratory is a U.S. Department of Energy Office of Science Laboratory operated under Contract No. DE-AC02-06CH11357. B.W.S. acknowledges support from the National Science Foundation (DMR-2124775).

Received: ((will be filled in by the editorial staff))

Revised: ((will be filled in by the editorial staff))

Published online: ((will be filled in by the editorial staff))

References

[1] D. M. Piper, T. Evans, K. Leung, T. Watkins, J. Olson, S. C. Kim, S. S. Han, V. Bhat, K. H. Oh, D. A. Buttry, *Nat. Commun.* **2015**, *6*, 1.
[2] F. Wu, N. Chen, R. Chen, Q. Zhu, G. Tan, L. Li, *Adv. Sci.* **2016**, *3*, 1500306.
[3] X. Liu, L. Zhang, H. Yu, J. Wang, J. Li, K. Yang, Y. Zhao, H. Wang, B. Wu, N. P. Brandon, *Adv. Energy Mater.* **2022**, 2200889.
[4] M. Park, H. Sun, H. Lee, J. Lee, J. Cho, *Adv. Energy Mater.* **2012**, *2*, 780.
[5] A. Bhowmik, M. Berecibar, M. Casas‐Cabanas, G. Csanyi, R. Dominko, K. Hermansson, M. R. Palacin, H. S. Stein, T. Vegge, *Adv. Energy Mater.* **2022**, *12*, 2102698.
[6] J. Amici, P. Asinari, E. Ayerbe, P. Barboux, P. Bayle‐Guillemaud, R. J. Behm, M. Berecibar, E. Berg, A. Bhowmik, S. Bodoardo, *Adv. Energy Mater.* **2022**, *12*, 2102785.
[7] E. Ayerbe, M. Berecibar, S. Clark, A. A. Franco, J. Ruhland, *Adv. Energy Mater.* **2022**, *12*, 2102696.
[8] A. Benayad, D. Diddens, A. Heuer, A. N. Krishnamoorthy, M. Maiti, F. L. Cras, M. Legallais, F. Rahmanian, Y. Shin, H. Stein, *Adv. Energy Mater.* **2022**, *12*, 2102678.
[9] Y. Huang, M. Zhong, Y. Huang, M. Zhu, Z. Pei, Z. Wang, Q. Xue, X. Xie, C. Zhi, *Nat. Commun.* **2015**, *6*, 1.
[10] M. Armand, J.-M. Tarascon, *Nature* **2008**, *451*, 652.
[11] D. Atkins, E. Ayerbe, A. Benayad, F. G. Capone, E. Capria, I. E. Castelli, I. Cekic‐Laskovic, R. Ciria, L. Dudy, K. Edström, *Adv. Energy Mater.* **2022**, *12*, 2102687.
[12] A. Rosenman, E. Markevich, G. Salitra, D. Aurbach, A. Garsuch, F. F. Chesneau, *Adv. Energy Mater.* **2015**, *5*, 1500212.
[13] Y. E. Durmus, H. Zhang, F. Baakes, G. Desmaizieres, H. Hayun, L. Yang, M. Kolek, V. Küpers, J. Janek, D. Mandler, *Adv. Energy Mater.* **2020**, *10*, 2000089.
[14] C. S. Li, Y. Sun, F. Gebert, S. L. Chou, *Adv. Energy Mater.* **2017**, *7*, 1700869.
[15] Q. Gu, J. A. Kimpton, H. E. Brand, Z. Wang, S. Chou, *Adv. Energy Mater.* **2017**, *7*, 1602831.
[16] A. Sepúlveda, J. Speulmanns, P. M. Vereecken, Sci. Technol. *Adv. Mater.* **2018**, *19*, 454.
[17] Y. Zhang, H. Sun, Y. Qiu, X. Ji, T. Ma, F. Gao, Z. Ma, B. Zhang, P. Hu, *Carbon* **2019**, *144*, 370.
[18] S. Stegmaier, R. Schierholz, I. Povstugar, J. Barthel, S. P. Rittmeyer, S. Yu, S. Wengert, S. Rostami, H. Kungl, K. Reuter, *Adv. Energy Mater.* **2021**, *11*, 2100707.
[19] Y. Song, L. Yang, W. Zhao, Z. Wang, Y. Zhao, Z. Wang, Q. Zhao, H. Liu, F. Pan, *Adv. Energy Mater.* **2019**, *9*, 1900671.
[20] D. Zhou, Y. B. He, R. Liu, M. Liu, H. Du, B. Li, Q. Cai, Q. H. Yang, F. Kang, *Adv. Energy Mater.* **2015**, *5*, 1500353.
[21] D. Fenton, *polymer* **1973**, *14*, 589.
[22] M. Armand, J. Chabagno, M. Duclot, St Andrews, Scotland **1978**, 20.
[23] H. Chen, D. Adekoya, L. Hencz, J. Ma, S. Chen, C. Yan, H. Zhao, G. Cui, S. Zhang, *Adv. Energy Mater.* **2020**, *10*, 2000049.
[24] J. Liang, D. Chen, K. Adair, Q. Sun, N. G. Holmes, Y. Zhao, Y. Sun, J. Luo, R. Li, L. Zhang, *Adv. Energy Mater.* **2021**, *11*, 2002455.
[25] N. Kamaya, K. Homma, Y. Yamakawa, M. Hirayama, R. Kanno, M. Yonemura, T. Kamiyama, Y. Kato, S. Hama, K. Kawamoto, *Nat. Mater.* **2011**, *10*, 682.

[26] Y. Kato, S. Hori, T. Saito, K. Suzuki, M. Hirayama, A. Mitsui, M. Yonemura, H. Iba, R. Kanno, *Nat. Energy* **2016**, *1*, 1.
[27] F. Zhao, J. Liang, C. Yu, Q. Sun, X. Li, K. Adair, C. Wang, Y. Zhao, S. Zhang, W. Li, *Adv. Energy Mater.* **2020**, *10*, 1903422.
[28] N. Sun, Y. Song, Q. Liu, W. Zhao, F. Zhang, L. Ren, M. Chen, Z. Zhou, Z. Xu, S. Lou, *Adv. Energy Mater.* **2022**, 2200682.
[29] Y. Chen, W. Li, C. Sun, J. Jin, Q. Wang, X. Chen, W. Zha, Z. Wen, *Adv. Energy Mater.* **2021**, *11*, 2002545.
[30] R. Rajagopalan, B. Chen, Z. Zhang, X. L. Wu, Y. Du, Y. Huang, B. Li, Y. Zong, J. Wang, G. H. Nam, *Adv. Mater.* **2017**, *29*, 1605694.
[31] D. Sun, X. Xue, Y. Tang, Y. Jing, B. Huang, Y. Ren, Y. Yao, H. Wang, G. Cao, *ACS Appl. Mater. Interfaces* **2015**, *7*, 28337.
[32] J. Fu, *Solid State Ion* **1997**, *96*, 195.
[33] Y. He, C. Lu, S. Liu, W. Zheng, J. Luo, *Adv. Energy Mater.* **2019**, *9*, 1901810.
[34] Y. Liu, C. Li, B. Li, H. Song, Z. Cheng, M. Chen, P. He, H. Zhou, *Adv. Energy Mater.* **2018**, *8*, 1702374.
[35] Y. Liu, Q. Sun, Y. Zhao, B. Wang, P. Kaghazchi, K. R. Adair, R. Li, C. Zhang, J. Liu, L.-Y. Kuo, *ACS Appl. Mater. Interfaces* **2018**, *10*, 31240.
[36] J. C. Bachman, S. Muy, A. Grimaud, H.-H. Chang, N. Pour, S. F. Lux, O. Paschos, F. Maglia, S. Lupart, P. Lamp, *Chem. Rev.* **2016**, *116*, 140.
[37] J. B. Goodenough, H.-P. Hong, J. Kafalas, *Mater. Res. Bull.* **1976**, *11*, 203.
[38] H.-P. Hong, *Mater. Res. Bull.* **1976**, *11*, 173.
[39] F. Mouahid, M. Zahir, P. Maldonado-Manso, S. Bruque, E. Losilla, M. Aranda, A. Rivera, C. Leonc, J. Santamariac, *J. Mater. Chem* **2001**, *11*, 3258.
[40] B. E. Francisco, C. R. Stoldt, J.-C. M'Peko, *Chem. Mater.* **2014**, *26*, 4741.
[41] D. Petit, P. Colomban, G. Collin, J. Boilot, *Mater. Res. Bull.* **1986**, *21*, 365.
[42] K. Nakano, N. Tanibata, H. Takeda, R. Kobayashi, M. Nakayama, N. Watanabe, *J. Phys. Chem. C* **2021**, *125*, 23604.
[43] Y. Noda, K. Nakano, H. Takeda, M. Kotobuki, L. Lu, M. Nakayama, *Chem. Mater.* **2017**, *29*, 8983.
[44] H. Xu, S. Wang, H. Wilson, F. Zhao, A. Manthiram, *Chem. Mater.* **2017**, *29*, 7206.
[45] Y. Li, M. Liu, K. Liu, C.-A. Wang, *J. Power Sources* **2013**, *240*, 50.
[46] Y. Noda, K. Nakano, M. Otake, R. Kobayashi, M. Kotobuki, L. Lu, M. Nakayama, *APL Mater.* **2018**, *6*, 060702.
[47] T. Pareek, B. Singh, S. Dwivedi, A. K. Yadav, S. Sen, P. Kumar, S. Kumar, *Electrochim. Acta* **2018**, *263*, 533.
[48] V. Ramar, S. Kumar, S. Sivakkumar, P. Balaya, *Electrochim. Acta* **2018**, *271*, 120.
[49] M. Catti, N. Morgante, R. Ibberson, *J. Solid State Chem.* **2000**, *2*, 340.
[50] P. Padma Kumar, S. Yashonath, *J. Phys. Chem. B* **2001**, *105*, 6785.
[51] M. Catti, A. Comotti, S. Di Blas, *Chem. Mater.* **2003**, *15*, 1628.
[52] K. Kamali, T. Ravindran, *J. Phys. Chem. A* **2016**, *120*, 1971.
[53] M. A. París, J. Sanz, *Phys. Rev. B* **2000**, *62*, 810.
[54] T. Zangina, J. Hassan, R. a. S. Azis, K. A. Matori, T. F. Khoon, M. A. Musa, *SN Appl. Sci.* **2019**, *1*, 1.
[55] E. R. Losilla, M. A. Aranda, M. Martinez-Lara, S. Bruque, *Chem. Mater.* **1997**, *9*, 1678.
[56] M. París, A. Martínez-Juárez, J. Iglesias, J. Rojo, J. Sanz, *Chem. Mater.* **1997**, *9*, 1430.
[57] C. R. Mariappan, C. Yada, F. Rosciano, B. Roling, *J. Power Sources* **2011**, *196*, 6456.
[58] Y. Nikodimos, M.-C. Tsai, L. H. Abrha, H. H. Weldeyohannis, S.-F. Chiu, H. K. Bezabh, K. N. Shitaw, F. W. Fenta, S.-H. Wu, W.-N. Su, *J. Mater. Chem. A* **2020**, *8*, 11302.
[59] J. Kang, H. Chung, C. Doh, B. Kang, B. Han, *J. Power Sources* **2015**, *293*, 11.

[60] H. Yamamoto, M. Tabuchi, T. Takeuchi, H. Kageyama, O. Nakamura, *J. Power Sources* **1997**, *68*, 397.
[61] S. Pershina, B. Antonov, A. Farlenkov, E. Vovkotrub, *J. Alloys Compd.* **2020**, *835*, 155281.
[62] M. Weiss, D. A. Weber, A. Senyshyn, J. r. Janek, W. G. Zeier, *ACS Appl. Mater. Interfaces* **2018**, *10*, 10935.
[63] A. Paolella, W. Zhu, G. L. Xu, A. La Monaca, S. Savoie, G. Girard, A. Vijh, H. Demers, A. Perea, N. Delaporte, *Adv. Energy Mater.* **2020**, *10*, 2001497.
[64] J. Yang, Z. Huang, P. Zhang, G. Liu, X. Xu, X. Yao, *ACS Appl. Energy Mater.* **2019**, *2*, 7299.
[65] Y.-C. Jung, M.-S. Park, C.-H. Doh, D.-W. Kim, *Electrochim. Acta* **2016**, *218*, 271.
[66] D. Bosubabu, J. Sivaraj, R. Sampathkumar, K. Ramesha, *ACS Appl. Energy Mater.* **2019**, *2*, 4118.
[67] W. Li, Q. Wang, J. Jin, Y. Li, M. Wu, Z. Wen, *Energy Storage Mater.* **2019**, *23*, 299.
[68] Q. Guo, Y. Han, H. Wang, S. Xiong, Y. Li, S. Liu, K. Xie, *ACS Appl. Mater. Interfaces* **2017**, *9*, 41837.
[69] C. Wang, Y. Yang, X. Liu, H. Zhong, H. Xu, Z. Xu, H. Shao, F. Ding, *ACS Appl. Mater. Interfaces* **2017**, *9*, 13694.
[70] G. Hou, X. Ma, Q. Sun, Q. Ai, X. Xu, L. Chen, D. Li, J. Chen, H. Zhong, Y. Li, *ACS Appl. Mater. Interfaces* **2018**, *10*, 18610.
[71] E. Zhao, F. Ma, Y. Guo, Y. Jin, *RSC Adv.* **2016**, *6*, 92579.
[72] H. Aono, N. Imanaka, G.-y. Adachi, Acc. *Chem. Res.* **1994**, *27*, 265.
[73] X. Lu, S. Wang, R. Xiao, S. Shi, H. Li, L. Chen, *Nano Energy* **2017**, *41*, 626.
[74] K. Kwatek, W. Ślubowska, J. Trébosc, O. Lafon, J. Nowiński, *J. Alloys Compd.* **2020**, *820*, 153072.
[75] K. Kwatek, M. Świniarski, J. Nowiński, *J. Solid State Chem.* **2018**, *265*, 381.
[76] K. Kwatek, J. Nowiński, *Solid State Ion* **2018**, *322*, 93.
[77] H. Aono, E. Sugimoto, Y. Sadaoka, N. Imanaka, G. y. Adachi, *J. Electrochem. Soc.* **1990**, *137*, 1023.
[78] H. Peng, H. Xie, J. B. Goodenough, *J. Power Sources* **2012**, *197*, 310.
[79] R. Kahlaoui, K. Arbi, I. Sobrados, R. Jimenez, J. Sanz, R. Ternane, *Inorg. Chem.* **2017**, *56*, 1216.
[80] K. Arbi, J. Rojo, J. Sanz, *J. Eur. Ceram. Soc.* **2007**, *27*, 4215.
[81] B. Lang, B. Ziebarth, C. Elsässer, *Chem. Mater.* **2015**, *27*, 5040.
[82] B. Zhang, Z. Lin, H. Dong, L.-W. Wang, F. Pan, *J. Mater. Chem. A* **2020**, *8*, 342.
[83] W. Xiao, J. Wang, L. Fan, J. Zhang, X. Li, *Energy Storage Mater.* **2019**, *19*, 379.
[84] H. Aono, E. Sugimoto, Y. Sadaaka, N. Imanaka, G. Adachi, *J. Electrochem. Soc.* **1989**, *136*.
[85] P. Birke, F. Salam, S. Döring, W. Weppner, *Solid State Ion* **1999**, *118*, 149.
[86] X. M. Wu, X. H. Li, Y. H. Zhang, M. F. Xu, Z. Q. He, *Mater. Lett* **2004**, *58*, 1227.
[87] X. He, Y. Zhu, Y. Mo, *Nat. Commun.* **2017**, *8*, 1.
[88] C. Wang, W. Ping, Q. Bai, H. Cui, R. Hensleigh, R. Wang, A. H. Brozena, Z. Xu, J. Dai, Y. Pei, *Science* **2020**, *368*, 521.
[89] B. Zhang, R. Tan, L. Yang, J. Zheng, K. Zhang, S. Mo, Z. Lin, F. Pan, *Energy Storage Mater.* **2018**, *10*, 139.
[90] K. Arbi, M. Hoelzel, A. Kuhn, F. García-Alvarado, J. Sanz, *Inorg. Chem.* **2013**, *52*, 9290.
[91] C. M. Chang, Y. I. Lee, S. H. Hong, H. M. Park, *J. Am. Ceram. Soc.* **2005**, *88*, 1803.
[92] K. Arbi, M. Lazarraga, D. Ben Hassen Chehimi, M. Ayadi-Trabelsi, J. Rojo, J. Sanz, *Chem. Mater.* **2004**, *16*, 255.
[93] D. Rettenwander, A. Welzl, S. Pristat, F. Tietz, S. Taibl, G. Redhammer, J. Fleig, *J. Mater. Chem. A* **2016**, *4*, 1506.

[94] H. R. Arjmandi, S. Grieshammer, *Phys. Chem. Chem. Phys* **2019**, *21*, 24232.
[95] V. Epp, Q. Ma, E.-M. Hammer, F. Tietz, M. Wilkening, *Phys. Chem. Chem. Phys* **2015**, *17*, 32115-32121.
[96] D. Pfalzgraf, D. Mutter, D. F. Urban, *Solid State Ion* **2021**, *359*, 115521.
[97] M. Monchak, T. Hupfer, A. Senyshyn, H. Boysen, D. Chernyshov, T. Hansen, K. G. Schell, E. C. Bucharsky, M. J. Hoffmann, H. Ehrenberg, *Inorg. Chem.* **2016**, *55*, 2941.
[98] K. Waetzig, A. Rost, U. Langklotz, B. Matthey, J. Schilm, *J. Eur. Ceram. Soc.* **2016**, *36*, 1995.
[99] C. Davis III, J. C. Nino, *J. Am. Ceram. Soc.* **2015**, *98*, 2422.
[100] K. Waetzig, A. Rost, C. Heubner, M. Coeler, K. Nikolowski, M. Wolter, J. Schilm, *J. Alloys Compd.* **2020**, *818*, 153237.
[101] L. Puech, C. Cantau, P. Vinatier, G. Toussaint, P. Stevens, *J. Power Sources* **2012**, *214*, 330.
[102] S. D. Jackman, R. A. Cutler, *J. Power Sources* **2012**, *218*, 65.
[103] C. Suryanarayana, E. Ivanov, V. Boldyrev, *Mater. Sci. Eng. A* **2001**, *304*, 151.
[104] C. Suryanarayana, *Prog. Mater Sci.* **2001**, *46*, 1.
[105] L. Ning, Y. Wu, S. Fang, E. Rahm, R. Holze, *J. Power Sources* **2004**, *133*, 229.
[106] E. Zhao, F. Ma, Y. Jin, K. Kanamura, *J. Alloys Compd.* **2016**, *680*, 646.
[107] H. Aono, E. Sugimoto, Y. Sadaoka, N. Imanaka, G.-y. Adachi, *Solid State Ion* **1990**, *40*, 38.
[108] R. Davis, B. McDermott, C. Koch, *Metall. Trans. A* **1988**, *19*, 2867.
[109] H. Morimoto, H. Awano, J. Terashima, Y. Shindo, S. Nakanishi, N. Ito, K. Ishikawa, S.-i. Tobishima, *J. Power Sources* **2013**, *240*, 636.
[110] Y. He, B. Li, H. Duan, S. Wang, S. Yin, Y. Hao, Y. Pan, K. Wu, *Ceram. Int.* **2020**, *46*, 14143.
[111] Z. Li, X. Zhao, *Funct. Mater. Lett.* **2019**, *12*, 1950047.
[112] Q. Xu, C.-L. Tsai, D. Song, S. Basak, H. Kungl, H. Tempel, F. Hausen, S. Yu, R.-A. Eichel, *J. Power Sources* **2021**, *492*, 229631.
[113] Q. Ma, Q. Xu, C. L. Tsai, F. Tietz, O. Guillon, *J. Am. Ceram. Soc.* **2016**, *99*, 410.
[114] X. Xu, Z. Wen, X. Yang, J. Zhang, Z. Gu, *Solid State Ion* **2006**, *177*, 2611.
[115] H. B. Lin, Y. M. Zhang, J. N. Hu, Y. T. Wang, L. D. Xing, M. Q. Xu, X. P. Li, W. S. Li, *J. Power Sources* **2014**, *257*, 37.
[116] X. Liu, J. Tan, J. Fu, R. Yuan, H. Wen, C. Zhang, *ACS Appl. Mater. Interfaces* **2017**, *9*, 11696.
[117] L. Dai, J. Wang, Z. Shi, L. Yu, J. Shi, *Ceram. Int.* **2021**, *47*, 11662.
[118] E.-j. Yi, K.-y. Yoon, H.-A. Jung, T. Nakayama, M.-j. Ji, H. Hwang, *Appl. Surf. Sci.* **2019**, *473*, 622.
[119] M. Kotobuki, M. Koishi, *Ceram. Int.* **2013**, *39*, 4645.
[120] M. Kotobuki, M. Koishi, *J. Asian Ceram. Soc.* **2019**, *7*, 69.
[121] P. Odenwald, Q. Ma, B. Davaasuren, E. Dashjav, F. Tietz, M. Wolff, W. Rheinheimer, S. Uhlenbruck, O. Guillon, D. Fattakhova‐Rohlfing, *ChemElectroChem* **2022,** *9*, e202101366.
[122] L. Huang, Z. Wen, M. Wu, X. Wu, Y. Liu, X. Wang, *J. Power Sources* **2011**, *196*, 6943.
[123] S. Duluard, A. Paillassa, L. Puech, P. Vinatier, V. Turq, P. Rozier, P. Lenormand, P.-L. Taberna, P. Simon, F. Ansart, *J. Eur. Ceram. Soc.* **2013**, *33*, 1145.
[124] Y. Huang, Y. Jiang, Y. Zhou, Z. Hu, X. Zhu, *ChemElectroChem* **2019**, *6*, 6016.
[125] K. M. Kim, D. O. Shin, Y.-G. Lee, *Electrochim. Acta* **2015,** *176*, 1364.
[126] C. Peng, Y. Kamiike, Y. Liang, K. Kuroda, M. Okido, *ACS Sustainable Chem. Eng.* **2019**, *7*, 10751.
[127] P.-Y. Yen, M.-L. Lee, D. H. Gregory, W.-R. Liu, *Ceram. Int.* **2020**, *46*, 20529.
[128] L. Hallopeau, D. Bregiroux, G. Rousse, D. Portehault, P. Stevens, G. Toussaint, C. Laberty-Robert, *J. Power Sources* **2018**, *378*, 48.

[129] S. He, Y. Xu, B. Zhang, X. Sun, Y. Chen, Y. Jin, *Chem. Eng. J.* **2018**, *345*, 483.
[130] Z. Kou, C. Miao, P. Mei, Y. Zhang, X. Yan, Y. Jiang, W. Xiao, *Ceram. Int.* **2020**, *46*, 9629.
[131] Z. Wang, Z. Kou, C. Miao, W. Xiao, *Ceram. Int.* **2019**, *45*, 14469.
[132] X. Lu, J. Hai, F. Zhang, X. Li, J. Li, *Ceram. Int.* **2022**, *48*, 2203.
[133] Z. Liu, X. Tian, M. Liu, S. Duan, Y. Ren, H. Ma, K. Tang, J. Shi, S. Hou, H. Jin, *Small* **2021**, *17*, 2002866.
[134] V. Siller, A. Morata, M. N. Eroles, R. Arenal, J. C. Gonzalez-Rosillo, J. M. L. del Amo, A. Tarancón, *J. Mater. Chem. A* **2021**, *9*, 17760.
[135] W. Lee, C. K. Lyon, J. H. Seo, R. Lopez‐Hallman, Y. Leng, C. Y. Wang, M. A. Hickner, C. A. Randall, E. D. Gomez, *Adv. Funct. Mater.* **2019**, *29*, 1807872.
[136] R. Pfenninger, M. Struzik, I. Garbayo, E. Stilp, J. L. Rupp, *Nat. Energy* **2019,** *4*, 475.
[137] X. Huang, Y. Lu, Z. Song, K. Rui, Q. Wang, T. Xiu, M. E. Badding, Z. Wen, *Energy Storage Mater.* **2019**, *22*, 207.
[138] I. Garbayo, M. Struzik, W. J. Bowman, R. Pfenninger, E. Stilp, J. L. Rupp, *Adv. Energy Mater.* **2018**, *8*, 1702265.
[139] M. Yu, S. Grasso, R. Mckinnon, T. Saunders, M. J. Reece, *Adv. Appl. Ceram.* **2017**, *116*, 24.
[140] Y. Liu, J. Liu, Q. Sun, D. Wang, K. R. Adair, J. Liang, C. Zhang, L. Zhang, S. Lu, H. Huang, *ACS Appl. Mater. Interfaces* **2019**, *11*, 27890.
[141] O. Guillon, J. Gonzalez‐Julian, B. Dargatz, T. Kessel, G. Schierning, J. Räthel, M. Herrmann, *Adv. Eng. Mater.* **2014**, *16*, 830.
[142] K. Arbi, W. Bucheli, R. Jiménez, J. Sanz, *J. Eur. Ceram. Soc.* **2015**, *35*, 1477.
[143] E. Zhao, Y. Guo, G. Xu, L. Yuan, J. Liu, X. Li, L. Yang, J. Ma, Y. Li, S. Fan, *J. Alloys Compd.* **2019**, *782*, 384.
[144] J. Gai, E. Zhao, F. Ma, D. Sun, X. Ma, Y. Jin, Q. Wu, Y. Cui, *J. Eur. Ceram. Soc.* **2018**, *38*, 1673.
[145] L. Dhivya, R. Murugan, *ACS Appl. Mater. Interfaces* **2014**, *6*, 17606.
[146] M. Liu, X. Li, X. Wang, R. Yu, M. Chen, Q. Lu, B. Lu, H. Shu, X. Yang, *J. Alloys Compd.* **2018**, *756*, 103.
[147] S. Li, Z. Huang, Y. Xiao, C. Sun, *Mater. Chem. Front.* **2021**, *5*, 5336.
[148] A. Kızılaslan, M. Kırkbınar, T. Cetinkaya, H. Akbulut, *Phys. Chem. Chem. Phys* **2020**, *22*, 17221.
[149] N. S. T. Do, D. M. Schaetzl, B. Dey, A. C. Seabaugh, S. K. Fullerton-Shirey, *J. Phys. Chem. C* **2012**, *116*, 21216.
[150] Y. Tominaga, K. Yamazaki, *Chem. Commun.* **2014**, *50*, 4448.
[151] L. Yang, Z. Wang, Y. Feng, R. Tan, Y. Zuo, R. Gao, Y. Zhao, L. Han, Z. Wang, F. Pan, *Adv. Energy Mater.* **2017**, *7*, 1701437.
[152] J. Kang, R. Gu, X. Guo, J. Li, H. Sun, L. Zhang, R. Jing, L. Jin, X. Wei, *Ceram. Int.* **2022**, *48*, 157.
[153] Z. Cai, Y. Huang, W. Zhu, R. Xiao, *Solid State Ion* **2020**, *354*, 115399.
[154] W. Ślubowska, L. Montagne, O. Lafon, F. Méar, K. Kwatek, *Nanomaterials* **2021**, *11*, 390.
[155] C. E. Athanasiou, M. Y. Jin, C. Ramirez, N. P. Padture, B. W. Sheldon, *Matter* **2020**, *3*, 212.
[156] H.-K. Tian, R. Jalem, B. Gao, Y. Yamamoto, S. Muto, M. Sakakura, Y. Iriyama, Y. Tateyama, *ACS Appl. Mater. Interfaces* **2020**, *12*, 54752.
[157] C.-Y. Yu, J. Choi, V. Anandan, J.-H. Kim, *J. Phys. Chem. C* **2020**, *124*, 14963.
[158] H.-S. Kim, Y. Oh, K. H. Kang, J. H. Kim, J. Kim, C. S. Yoon, *ACS Appl. Mater. Interfaces* **2017**, *9*, 16063.

[159] Y. Jin, X. Zong, X. Zhang, C. Liu, D. Li, Z. Jia, G. Li, X. Zhou, J. Wei, Y. Xiong, *J. Power Sources* **2021**, *501*, 230027.
[160] J.-Y. Liang, X.-X. Zeng, X.-D. Zhang, T.-T. Zuo, M. Yan, Y.-X. Yin, J.-L. Shi, X.-W. Wu, Y.-G. Guo, L.-J. Wan, *J. Am. Chem. Soc.* **2019**, *141*, 9165.
[161] Z. Yang, H. Yuan, C. Zhou, Y. Wu, W. Tang, S. Sang, H. Liu, *Chem. Eng. J.* **2020**, *392*, 123650.
[162] S. Yu, S. Schmohl, Z. Liu, M. Hoffmeyer, N. Schön, F. Hausen, H. Tempel, H. Kungl, H. D. Wiemhöfer, R. A. Eichel, *J. Mater. Chem. A* **2019**, *7*, 3882.
[163] A. Aboulaich, R. Bouchet, G. Delaizir, V. Seznec, L. Tortet, M. Morcrette, P. Rozier, J. M. Tarascon, V. Viallet, M. Dollé, *Adv. Energy Mater.* **2011**, *1*, 179.
[164] S. Ohta, J. Seki, Y. Yagi, Y. Kihira, T. Tani, T. Asaoka, *J. Power Sources* **2014**, *265*, 40.
[165] Z. Gao, H. Sun, L. Fu, F. Ye, Y. Zhang, W. Luo, Y. Huang, *Adv. Mater.* **2018**, *30*, 1705702.
[166] K. Nagata, T. Nanno, *J. Power Sources* **2007**, *174*, 832.
[167] T. Kato, R. Yoshida, K. Yamamoto, T. Hirayama, M. Motoyama, W. C. West, Y. Iriyama, *J. Power Sources* **2016**, *325*, 584.
[168] R. Chen, C. Yao, Q. Yang, H. Pan, X. Yu, K. Zhang, H. Li, *ACS Appl. Mater. Interfaces* **2021**, *13*, 18743.
[169] Z. Liu, Y. Qi, Y. Lin, L. Chen, P. Lu, L. Chen, *J. Electrochem. Soc.* **2016**, *163*, A592.
[170] J. Zhu, J. Zhao, Y. Xiang, M. Lin, H. Wang, B. Zheng, H. He, Q. Wu, J. Y. Huang, Y. Yang, *Chem. Mater.* **2020**, *32*, 4998.
[171] Y. Wang, G. Wang, P. He, J. Hu, J. Jiang, L.-Z. Fan, *Chem. Eng. J.* **2020**, *393*, 124705.
[172] Y. Jin, C. Liu, X. Zong, D. Li, M. Fu, S. Tan, Y. Xiong, J. Wei, *J. Power Sources* **2020**, *460*, 228125.
[173] J. Tang, L. Wang, C. Tian, T. Huang, L. Zeng, A. Yu, *J. Power Sources* **2021**, *515*, 230639.
[174] V. Nilsson, A. Kotronia, M. Lacey, K. Edström, P. Johansson, *ACS Appl. Energy Mater.* **2019**, *3*, 200.
[175] W. Cao, Y. Yang, J. Deng, Y. Li, C. Cui, T. Zhang, *Mater. Today Energy* **2021**, *22*, 100875.
[176] Z. Chen, G. T. Kim, J. K. Kim, M. Zarrabeitia, M. Kuenzel, H. P. Liang, D. Geiger, U. Kaiser, S. Passerini, *Adv. Energy Mater.* **2021**, *11*, 2101339.
[177] Q. Cheng, A. Li, N. Li, S. Li, A. Zangiabadi, W. Huang, A. C. Li, T. Jin, Q. Song, W. Xu, *Joule* **2019**, *3*, 1510.
[178] X. Hao, Q. Zhao, S. Su, S. Zhang, J. Ma, L. Shen, Q. Yu, L. Zhao, Y. Liu, F. Kang, *Adv. Energy Mater.* **2019**, *9*, 1901604.
[179] L. Yang, Y. Song, H. Liu, Z. Wang, K. Yang, Q. Zhao, Y. Cui, J. Wen, W. Luo, F. Pan, *Small Methods* **2020**, *4*, 1900751.
[180] Y. Li, X. Feng, D. Ren, M. Ouyang, L. Lu, X. Han, *ACS Appl. Mater. Interfaces* **2019**, *11*, 46839.
[181] R. Chen, A. M. Nolan, J. Lu, J. Wang, X. Yu, Y. Mo, L. Chen, X. Huang, H. Li, *Joule* **2020**, *4*, 812.
[182] L. He, W.-H. Liang, J.-H. Cao, D.-Y. Wu, *ACS Appl. Energy Mater.* **2022**,*5(4)*, 5277.
[183] D. Li, L. Chen, T. Wang, L.-Z. Fan, *ACS Appl. Mater. Interfaces* **2018**, *10*, 7069.
[184] L. Zhu, Y. Wang, Y. Wu, W. Feng, Z. Liu, W. Tang, X. Wang, Y. Xia, *Adv. Funct. Mater.* **2022**, 2201136.
[185] L.-Z. Fan, H. He, C.-W. Nan, *Nat. Rev. Mater.* **2021**, *6*, 1003-1019.
[186] W. Liu, S. W. Lee, D. Lin, F. Shi, S. Wang, A. D. Sendek, Y. Cui, *Nat. Energy* **2017,** *2*, 17035.
[187] G. Wang, P. He, L.-Z. Fan, *Adv. Funct. Mater.* **2021**, *31*, 2007198.
[188] X. Yu, A. Manthiram, *Energy Stor. Mater.* **2021**, *34*, 282.

[189] L. Chen, Y. Li, S.-P. Li, L.-Z. Fan, C.-W. Nan, J. B. Goodenough, *Nano Energy* **2018**, *46*, 176.
[190] S. Liu, W. Liu, D. Ba, Y. Zhao, Y. Ye, Y. Li, J. Liu, *Adv. Mater.* **2022**, 2110423.
[191] H. Huo, Y. Chen, J. Luo, X. Yang, X. Guo, X. Sun, *Adv. Energy Mater.* **2019**, *9*, 1804004.
[192] H. Kitaura, H. Zhou, *Adv. Energy Mater.* **2012**, *2*, 889.
[193] X. Yu, A. Manthiram, *ACS Appl. Energy Mater.* **2020**, *3*, 2916.
[194] Y. Lin, K. Liu, C. Xiong, M. Wu, T. Zhao, *J. Mater. Chem. A* **2021**, *9*, 9665.
[195] G. Wang, H. Liu, Y. Liang, C. Wang, L.-Z. Fan, *Energy Stor. Mater.* **2022**, *45*, 1212.
[196] S. Li, G. Sun, M. He, H. Li, *ACS Appl. Mater. Interfaces* **2022**.
[197] D. Lei, Y.-B. He, H. Huang, Y. Yuan, G. Zhong, Q. Zhao, X. Hao, D. Zhang, C. Lai, S. Zhang, *Nat. Commun.* **2019**, *10*, 1.
[198] W. Liu, C. Yi, L. Li, S. Liu, Q. Gui, D. Ba, Y. Li, D. Peng, J. Liu, *Angew. Chem.* **2021**, *133*, 13041.
[199] J. Li, Z. Wang, Z. Zhou, C. Li, Z. He, J. Zheng, Y. Li, J. Mao, K. Dai, C. Yan, *J. Power Sources* **2022**, *544*, 231891.
[200] K. Yang, L. Chen, J. Ma, C. Lai, Y. Huang, J. Mi, J. Biao, D. Zhang, P. Shi, H. Xia, *Angew. Chem. Int. Ed.* **2021**, *60*, 24668.
[201] Q. Zhou, J. Ma, S. Dong, X. Li, G. Cui, *Adv. Mater.* **2019**, *31*, 1902029.
[202] J. Bae, Y. Li, F. Zhao, X. Zhou, Y. Ding, G. Yu, *Energy Stor. Mater.* **2018**, *15*, 46.
[203] Y. Jin, X. Zong, X. Zhang, Z. Jia, H. Xie, Y. Xiong, *Energy Stor. Mater.* **2022**, *49*, 433.
[204] N. C. Rosero-Navarro, R. Kajiura, A. Miura, K. Tadanaga, *ACS Appl. Energy Mater.* **2020**, *3*, 11260.
[205] X. C. Chen, X. Liu, A. Samuthira Pandian, K. Lou, F. M. Delnick, N. J. Dudney, *ACS Energy Lett.* **2019**, *4*, 1080.
[206] W. J. Hyun, C. M. Thomas, N. S. Luu, M. C. Hersam, *Adv. Mater.* **2021**, *33*, 2007864.
[207] B. Li, C. Wang, Y. Zhang, Y. Wang, *Green Energy Environ.* **2021**, *6*, 253.
[208] A. J. Bhattacharyya, J. Maier, *Adv. Mater.* **2004**, *16*, 811.
[209] X. Song, C. Wang, J. Chen, S. Xin, D. Yuan, Y. Wang, K. Dong, L. Yang, G. Wang, H. Zhang, *Adv. Funct. Mater.* **2022**, *32*, 2108706.
[210] J. Fu, *Solid State Ion* **1997**, *104*, 191.
[211] Y. Inaguma, C. Liquan, M. Itoh, T. Nakamura, T. Uchida, H. Ikuta, M. Wakihara, *Solid State Commun* **1993**, *86*, 689.
[212] H. W. Buschmann, J. Doelle, S. Berendts, A. Kuhn, P. Bottke, M. Wilkening, P. Heitjans, A. Senyshyn, H. Ehrenberg, A. Lotnyk, V. Duppel, L. Kienle, J. Janek, Phys. Chem. Chem. Phys. **2011**, *13 43*, 19378.
[213] P. G. Bruce, A. West, *J. Electrochem. Soc.* **1983**, *130*, 662.
[214] W. Wang, E. Yi, A. J. Fici, R. M. Laine, J. Kieffer, *J. Phys. Chem. C* **2017**, *121*, 2563.
[215] H. Zhang, C. Liu, L. Zheng, F. Xu, W. Feng, H. Li, X. Huang, M. Armand, J. Nie, Z. Zhou, *Electrochim. Acta* **2014**, *133*, 529.
[216] Y. Seino, T. Ota, K. Takada, A. Hayashi, M. Tatsumisago, *Energy Environ. Sci.* **2014**, *7*, 627.
[217] N. Suzuki, T. Inaba, T. Shiga, *Thin Solid Films* **2012**, *520*, 1821.
[218] J. Bates, N. Dudney, B. Neudecker, A. Ueda, C. Evans, *Solid State Ion* **2000**, *135*, 33.

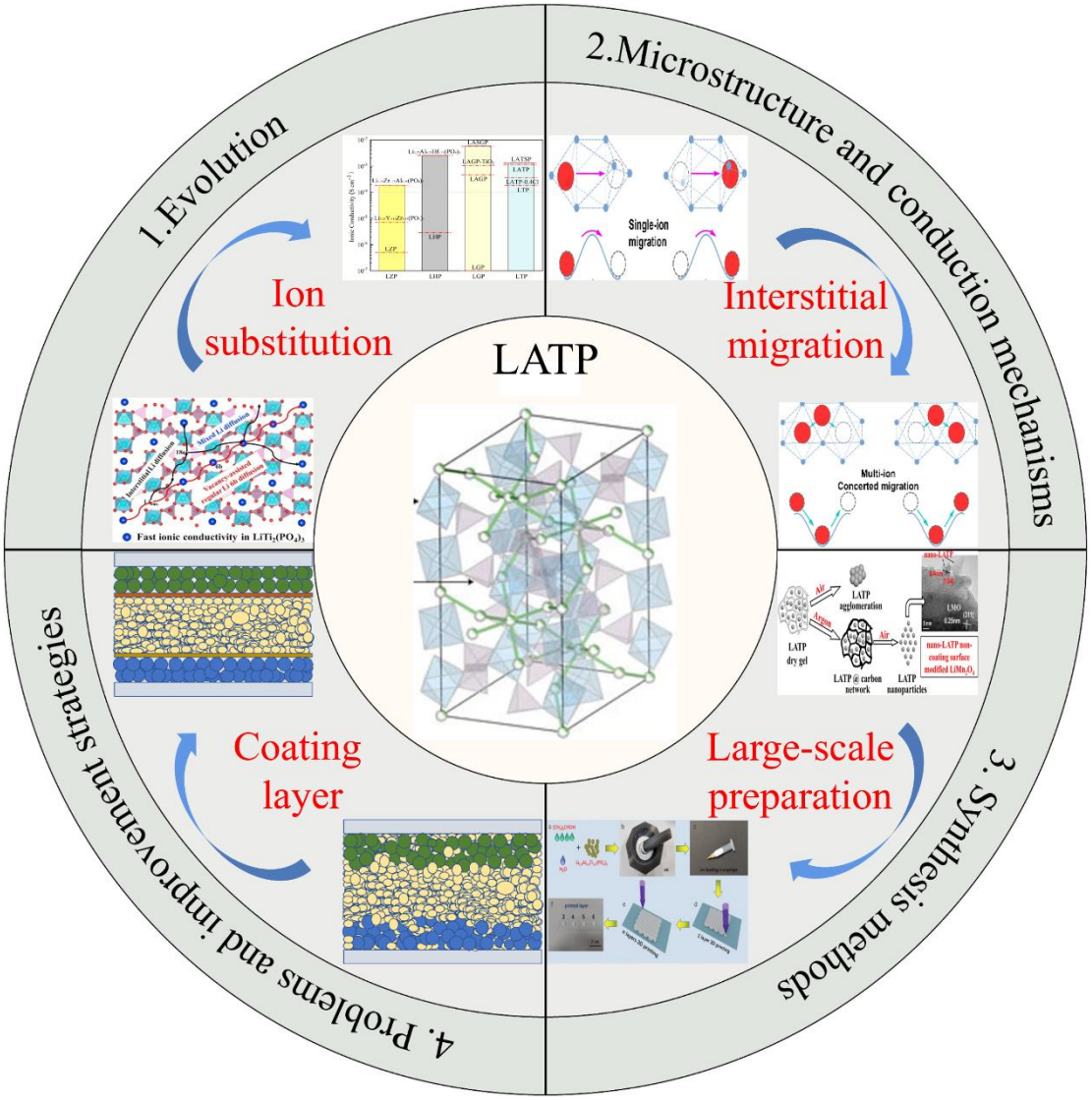

Figure 1. Schematic of the structure of this review. Reproduced with permission.[73] Copyright 2017, Elsevier. Reproduced with permission.[87] Copyright 2017, Nature Communications. Reproduced with permission.[116] Copyright 2017, American Chemical Society. Reproduced with permission.[133] Copyright 2021, Wiley-VCH.

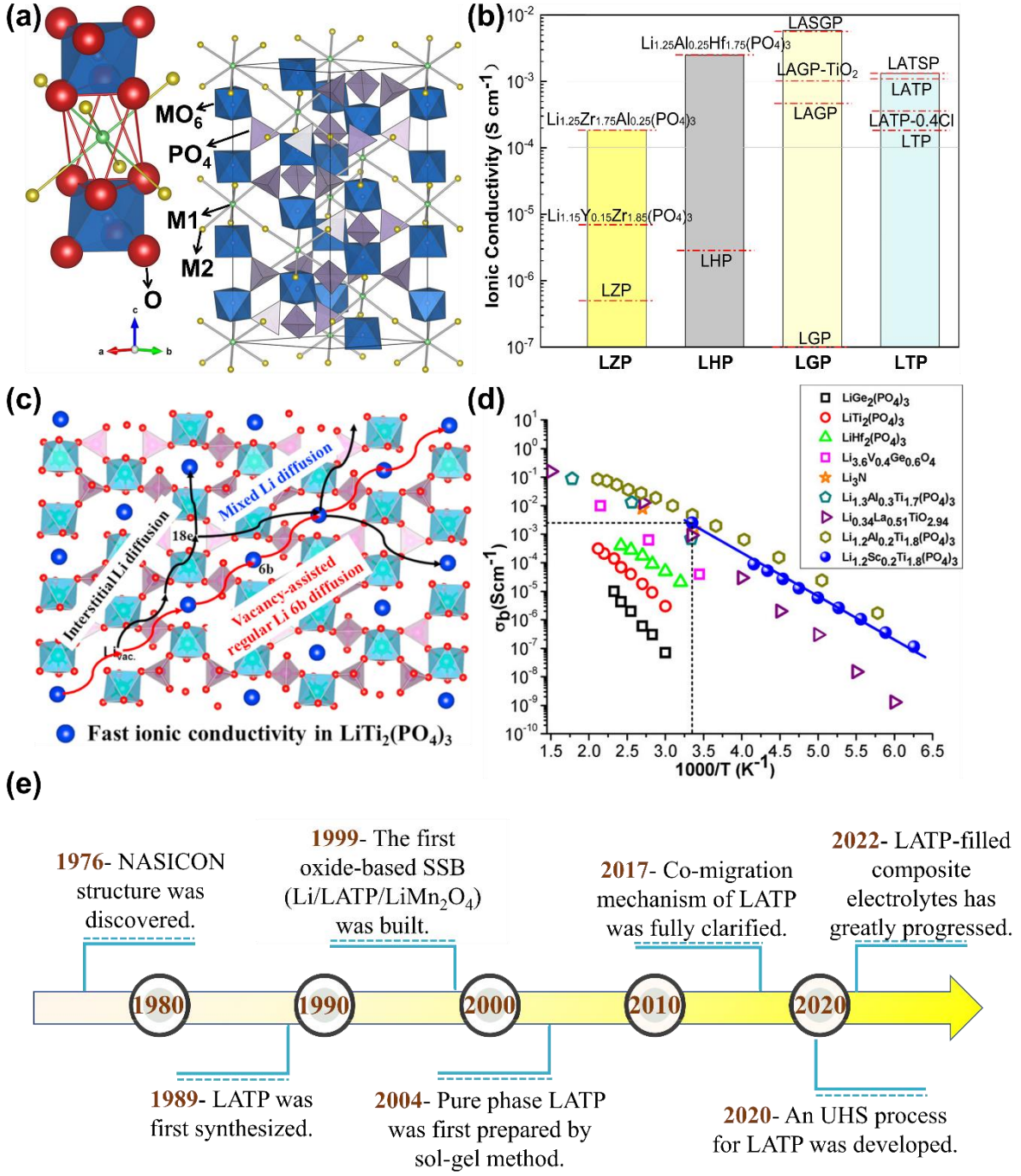

Figure 2. a) NASICON structure and the transport paths of Li ions. Reproduced with permission.[40] Copyright 2014, American Chemical Society. b) The evolution of the ionic conductivity of Li-based NASICON-type electrolyte over the years. c) Li ionic diffusions in LTP structure. Reproduced with permission.[73] Copyright 2017, Elsevier. d) The ionic conductivity of the $Li_{1+x}Ti_{2-x}M_x(PO_4)_3$ electrolyte. Reproduced with permission.[79] Copyright 2012, American Chemical Society. e) The evolution of LATP.

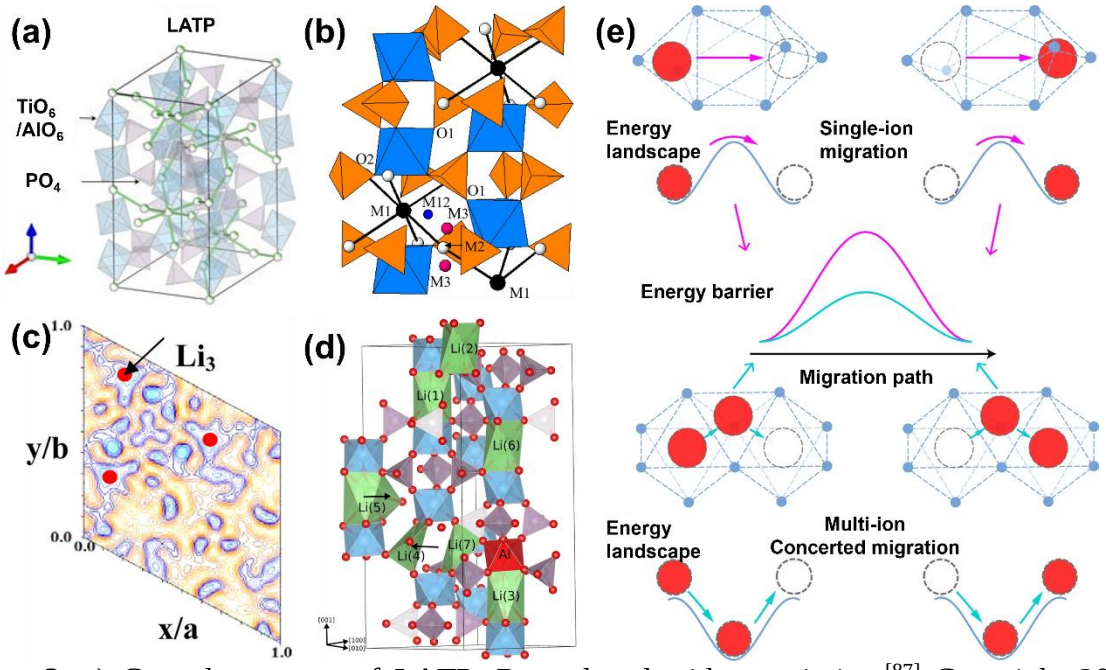

Figure 3. a) Crystal structure of LATP. Reproduced with permission.[87] Copyright 2017, Nature Communications. b) Schematic illustration of the NASICON-type structure distributed along the M1, M2, M3 sites of the Li^+ conduction pathway. Reproduced with permission.[90] Copyright 2013, American Chemical Society. c) Fourier map differences from ND patterns of the LATP sample recorded at 5 K. Reproduced with permission.[90] Copyright 2013, American Chemical Society. d) Li migration path of LATP. Reproduced with permission.[81] Copyright 2015, American Chemical Society. e) Schematic diagram of single ion migration and multi-ion co-migration. Reproduced with permission.[87] Copyright 2017, Nature Communications.

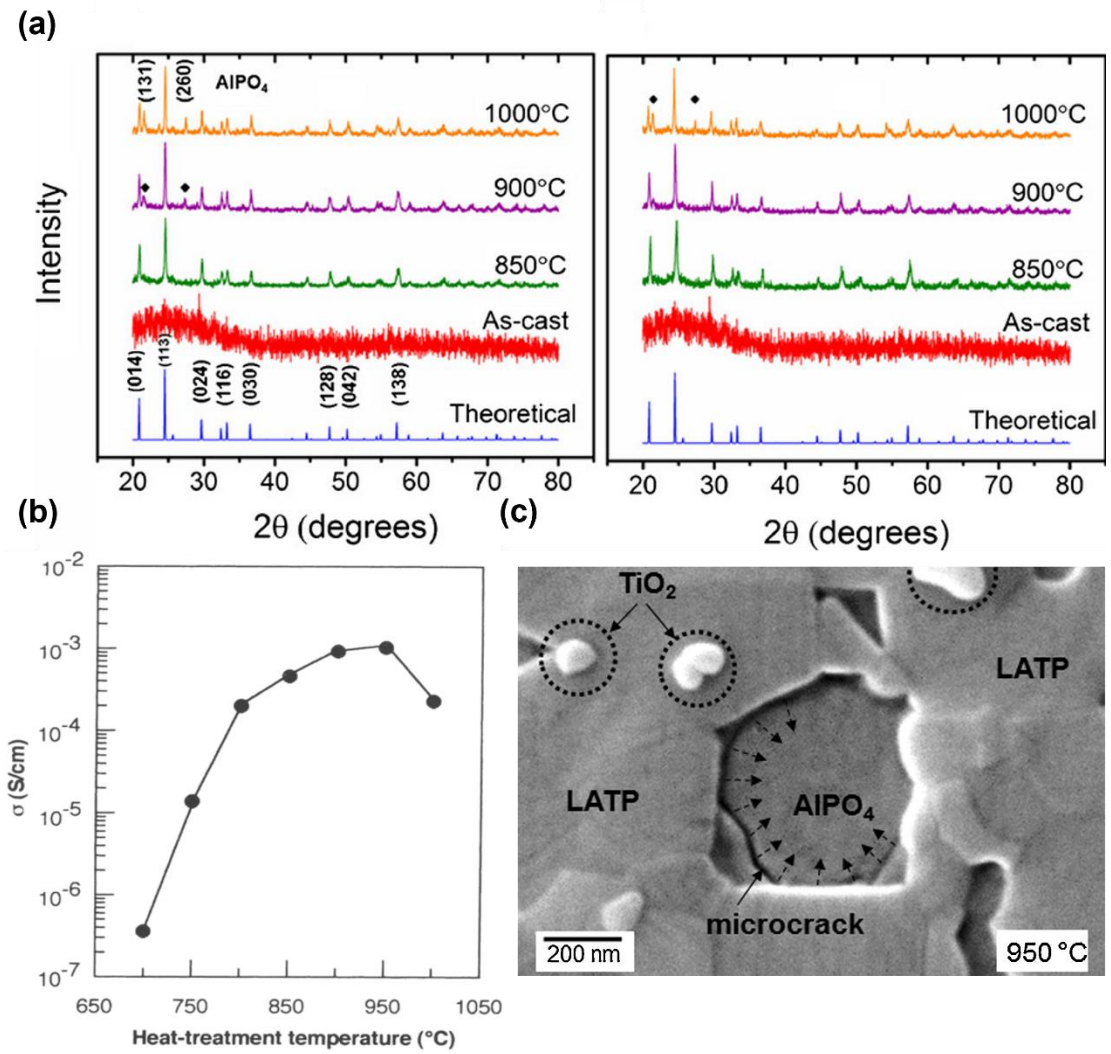

Figure 4. a) XRD patterns of LATP crystallized at different temperatures via conventional heating (left) and microwave heating (right). Reproduced with permission.[99] Copyright 2015, Wiley-VCH. b) Variation of LATP ionic conductivity at RT with heat-treatment temperature. Reproduced with permission.[32] Copyright 1997, Elsevier. c) Detailed microstructure of LATP sintered at 950 °C with hypothetical secondary phases of $AlPO_4$ and TiO_2, and microcracks in the $AlPO_4$ phase with hypothetical stress directions (with arrows). Reproduced with permission.[98] Copyright 2016, Elsevier.

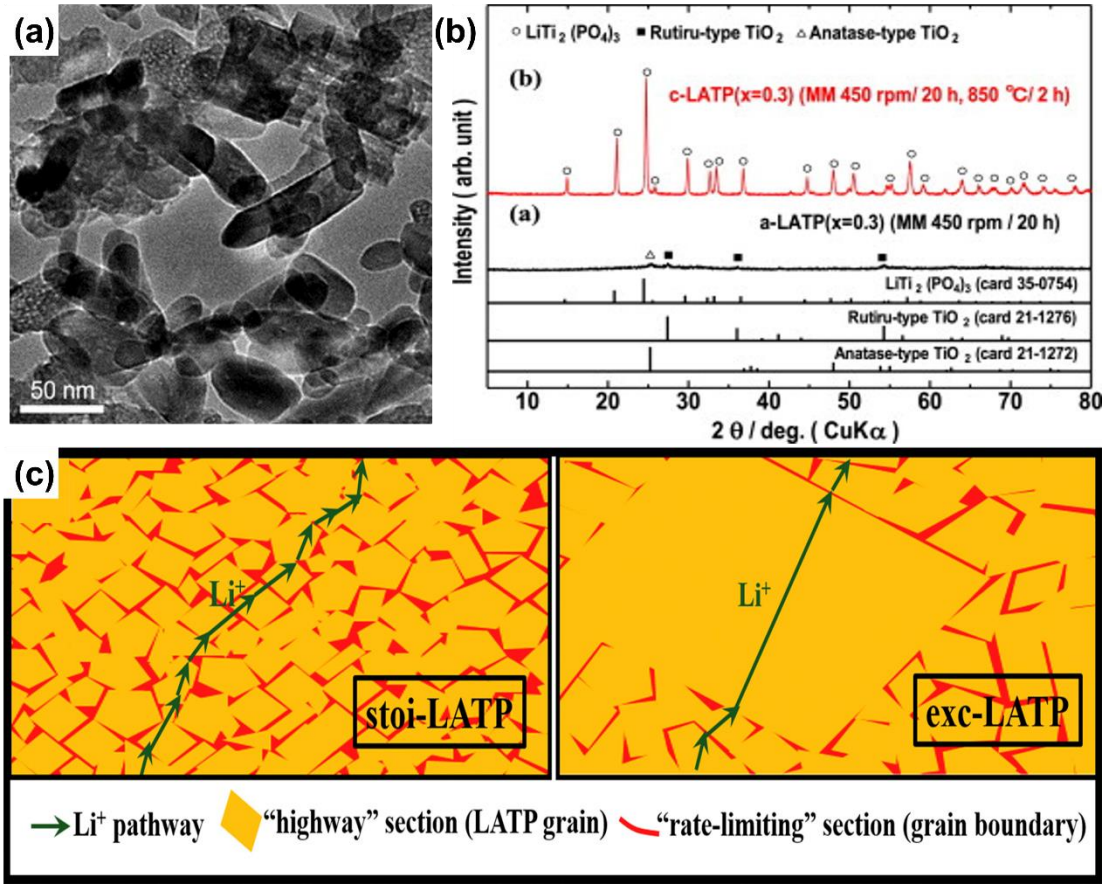

Figure 5. a) TEM image showing the particle size of the LATP powders prepared by mechanical milling for 40 h. Reproduced with permission.[114] Copyright 2006, Elsevier. b) XRD patterns of a-LATP (x= 0.3) powder obtained by mechanical milling treatment (top) and c-LATP (x = 0.3) powder obtained by heat treatment of a-LATP (x = 0.3) powder (bottom). Reproduced with permission.[109] Copyright 2013, Elsevier. c) Schematic illustration of the Li ion transportation for stoi-LATP and exc-LATP. Reproduced with permission.[112] Copyright 2021, Elsevier.

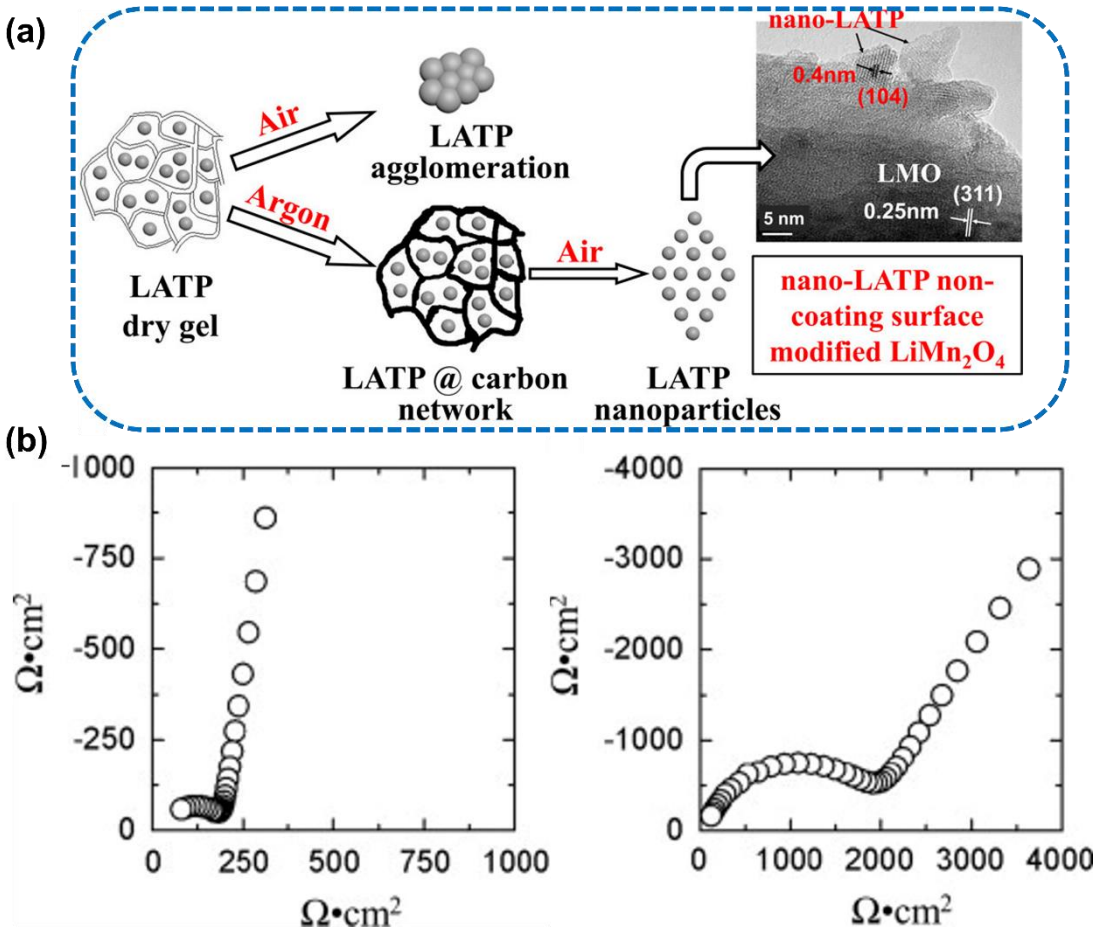

Figure 6. a) Diagram of the preparation of the LATP by conventional calcination and modified two-step calcination sol–gel method, with the SEM images of the prepared LATP. Reproduced with permission.[116] Copyright 2017, American Chemical Society. b) Complex impedance plots of the LATP obtained by the sol–gel method using $Al(C_3H_7O)_3$ (left) and $Al(NO_3)_3$ (right) as Al sources. Reproduced with permission.[119] Copyright 2013, Elsevier.

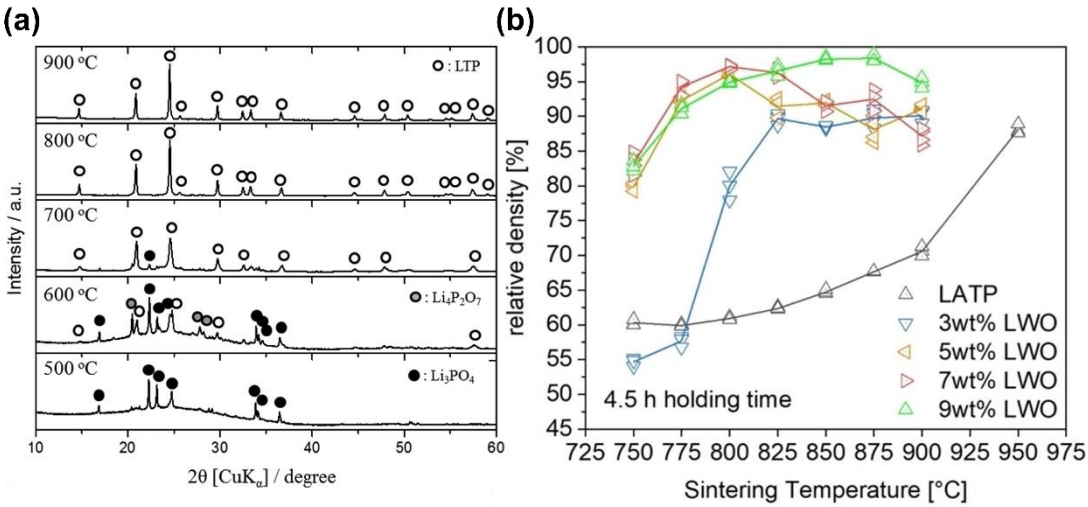

Figure 7. a) XRD patterns of the precursor powders calcined at various temperatures. Reproduced under terms of the CC-BY license.[120] Copyright 2019, M Kotobuki, M Koishi, published by Taylor & Francis. b) Influence of different sintering temperature and varying amounts of Li_2WO_4 additive on relative densities. Reproduced with permission.[121] Copyright 2022, Wiley-VCH.

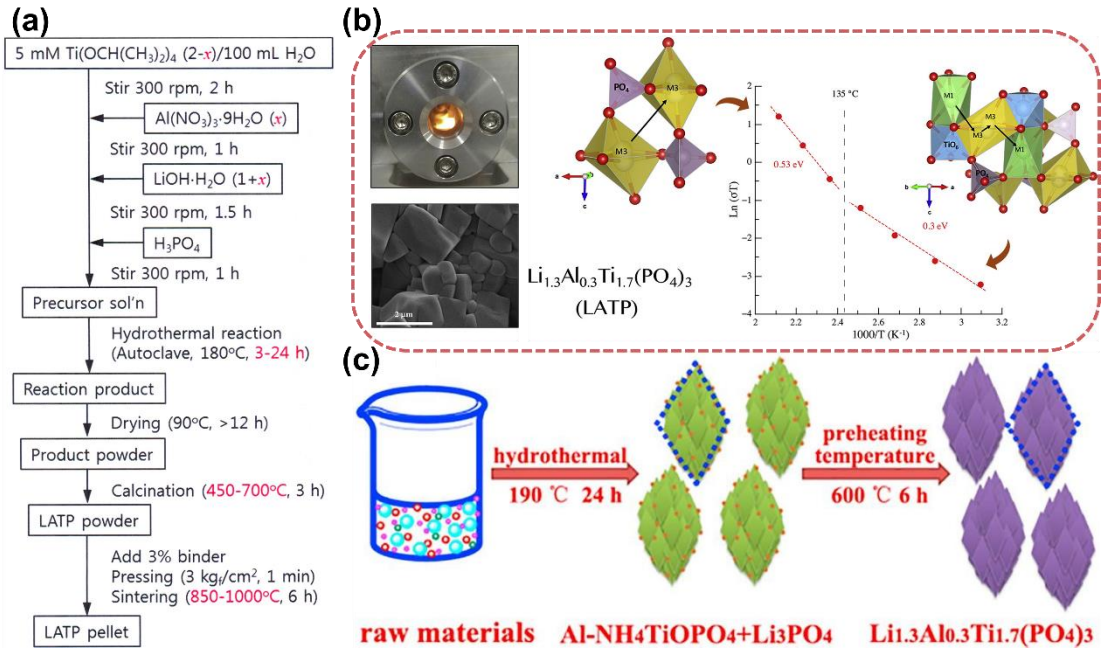

Figure 8. a) Hydrothermal synthesis procedure for LATP. Reproduced with permission.[125] Copyright 2015, Elsevier. b) SEM images, Arrhenius plot of the conductivity of LATP at 890 °C. Reproduced with permission.[128] Copyright 2018, Elsevier. c) Schematic illustration of the LATP prepared by hydrothermal process. Reproduced with permission.[129] Copyright 2018, Elsevier.

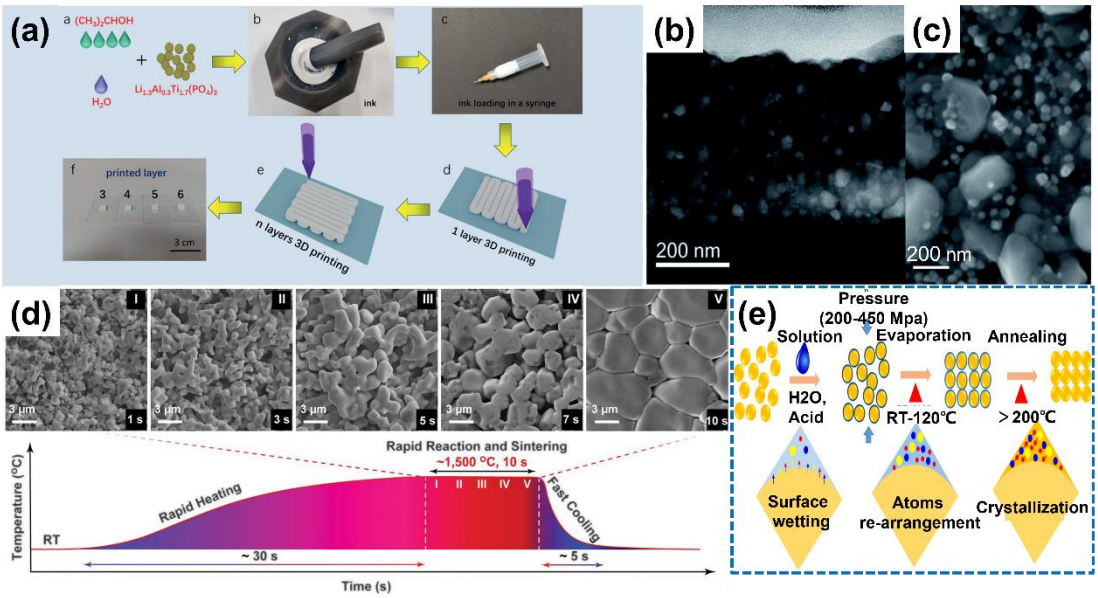

Figure 9. a) Schematic illustration of the DIW synthesis procedure for LATP. Reproduced with permission.[133] Copyright 2021, Wiley-VCH. b,c) SEM images of the LATP obtained by PLD. Reproduced under terms of the CC-BY license.[134] Copyright 2021, Siller, V., A. Morata, M. N. Eroles, R. Arenal, J. C. Gonzalez-Rosillo, J. M. L. del Amo, and A. Tarancón, published by Royal Society of Chemistry. d) Temperature rendition diagram of the UHS process. Reproduced with permission.[88] Copyright 2020, Science. e) Schematic illustration of the cold sintering process. Reproduced with permission.[140] Copyright 2019, American Chemical Society.

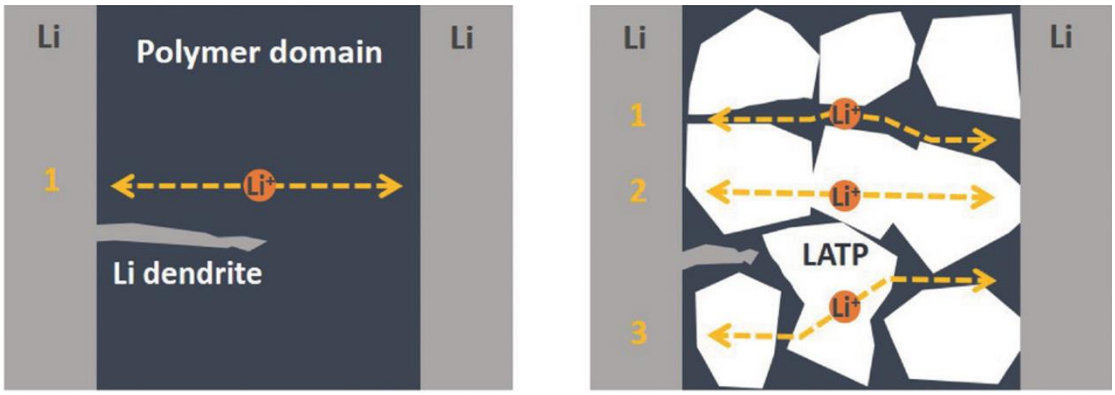

Figure 10. Schematic illustration of Li ion and electron transfer pathways via without additives (left) and with additives (right). Reproduced with permission.[151] Copyright 2017, Wiley-VCH.

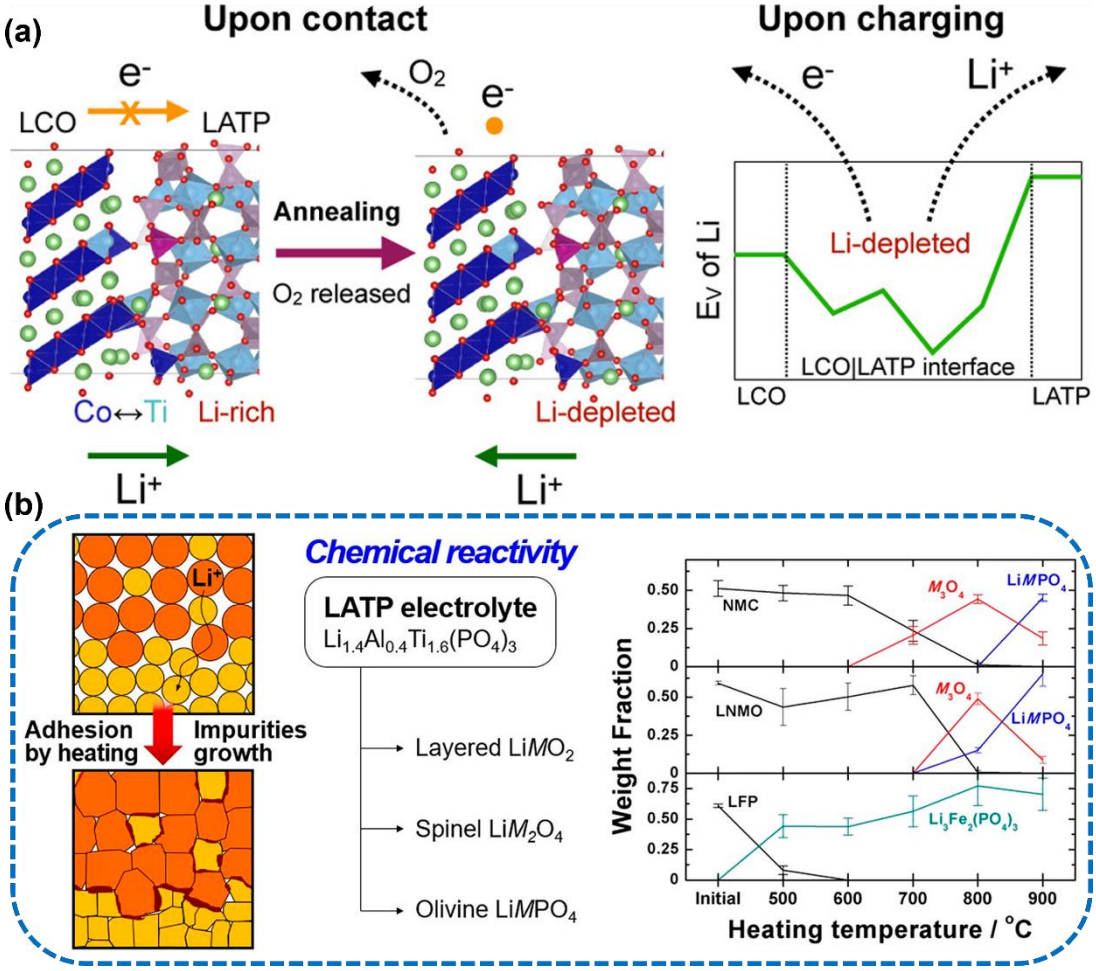

Figure 11. a) Schematic illustration of Li ion and electron transfer at the LATP/LCO interface upon contact, after annealing, and upon charging. Reproduced with permission.[156] Copyright 2020, Chan-Yeop Yu, Junbin Choi, Venkataramani Anandan, and Jung-Hyun Kim, published by American Chemical Society. b) Chemical reaction mechanism of $Li_{1.4}Al_{0.4}Ti_{1.6}(PO_4)_3$ SSE with various SSB cathode materials at high temperature. Reproduced with permission.[157] Copyright 2020, American Chemical Society.

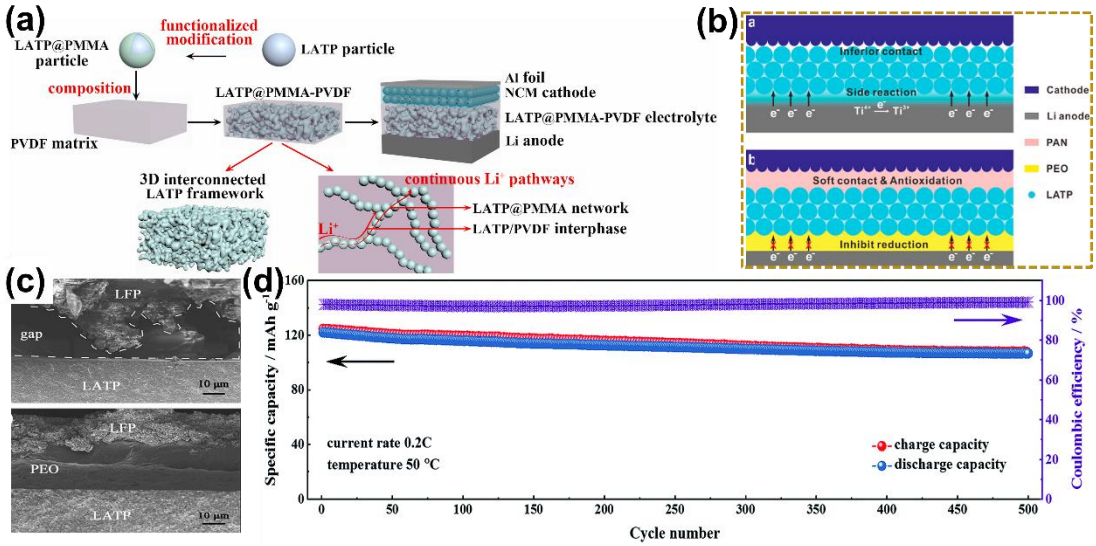

Figure 12. a) Schematic illustration of the synthesis process and the functional mechanism of the 3D structural composite electrolyte. Reproduced with permission.[159] Copyright 2021, Elsevier. b) Schematic illustration of pristine LATP and DPCE (PAN coating). Reproduced with permission.[160] Copyright 2019, American Chemical Society. c) SEM images of the LFP/LATP cross sections without (above) and with (bottom) a PEO interlayer. Reproduced with permission.[161] Copyright 2020, Elsevier. d) Cycling performances of the Li/SSE/$Li_3V_2(PO_4)_3$/CNT SSB at 50 °C and a current rate of 0.2 C. Reproduced under terms of the CC-BY license.[162] Copyright 2019, Yu, S., S. Schmohl, Z. Liu, M. Hoffmeyer, N. Schön, F. Hausen, H. Tempel, H. Kungl, H. D. Wiemhöfer, and R. A. Eichel, published by Royal Society of Chemistry.

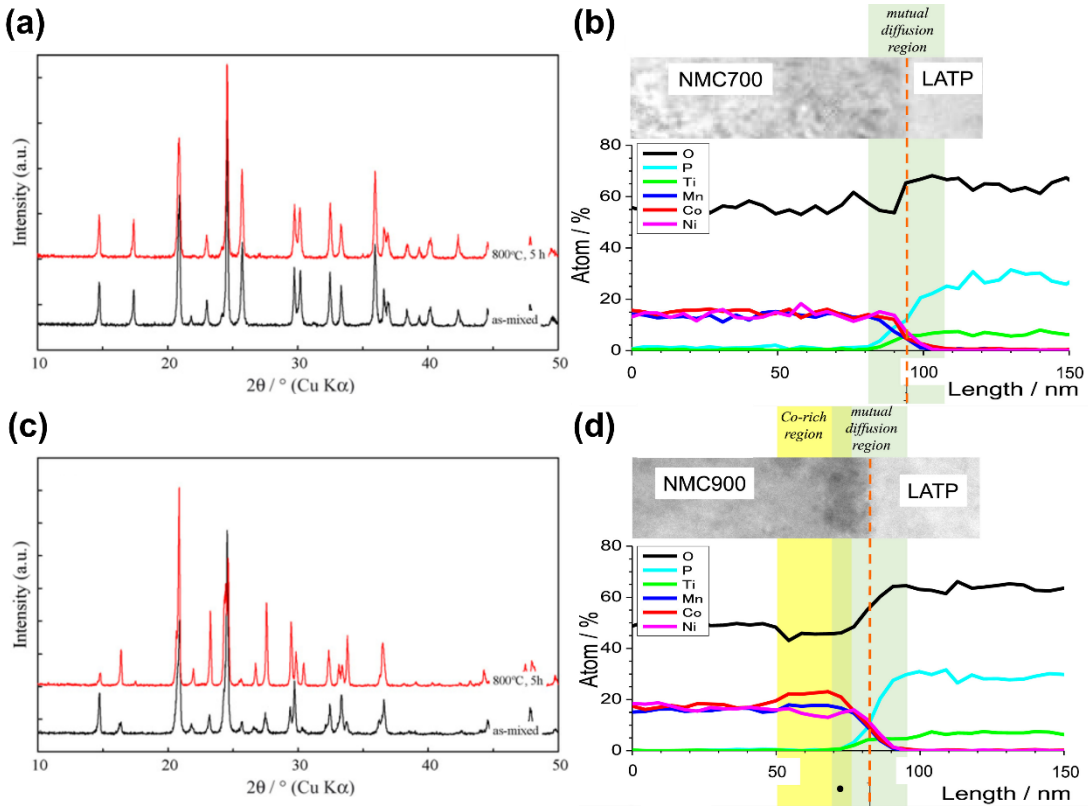

Figure 13. XRD patterns of a) $LiCoPO_4$/LATP and c) $Li_3Fe_2(PO_4)_3$/LATP. Reproduced with permission.[166] Copyright 2007, Elsevier. EDX line profiles of O, P, Ti, Mn, Ni, and Co around the b) NMC-700/LATP and d) NMC-900/LATP sheet interface. Reproduced with permission.[167] Copyright 2016, Elsevier.

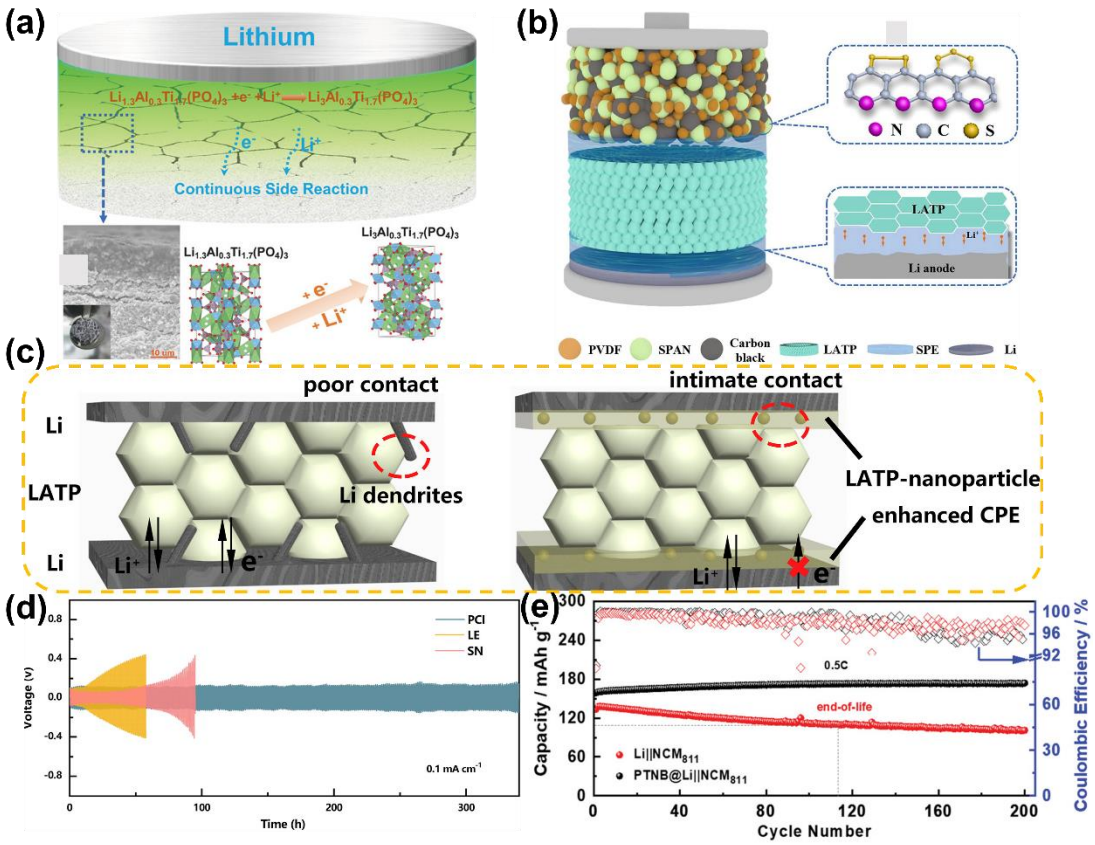

Figure 14. a) Dynamic electron/ion transport processes at the LATP negative interface. Reproduced with permission.[169] Copyright 2020, American Chemical Society. b) Schematic diagram of solid-state SPAN battery. Reproduced with permission.[171] Copyright 2020, Elsevier. c) Schematic illustration of the interface evolution between LATP and Li. Reproduced with permission.[172] Copyright 2020, Elsevier. d) Long cycling performance of Li/PCI/LATP/PCI/Li symmetric cells at 0.1 C. Reproduced with permission.[175] Copyright 2021, Elsevier. e) Cycling performance of Li/PTNB@LATP/$LiNi_{0.8}Co_{0.1}Mn_{0.1}O_2$ SSB at 0.5 C and 20 °C. Reproduced with permission.[176] Copyright 2021, Wiley-VCH.

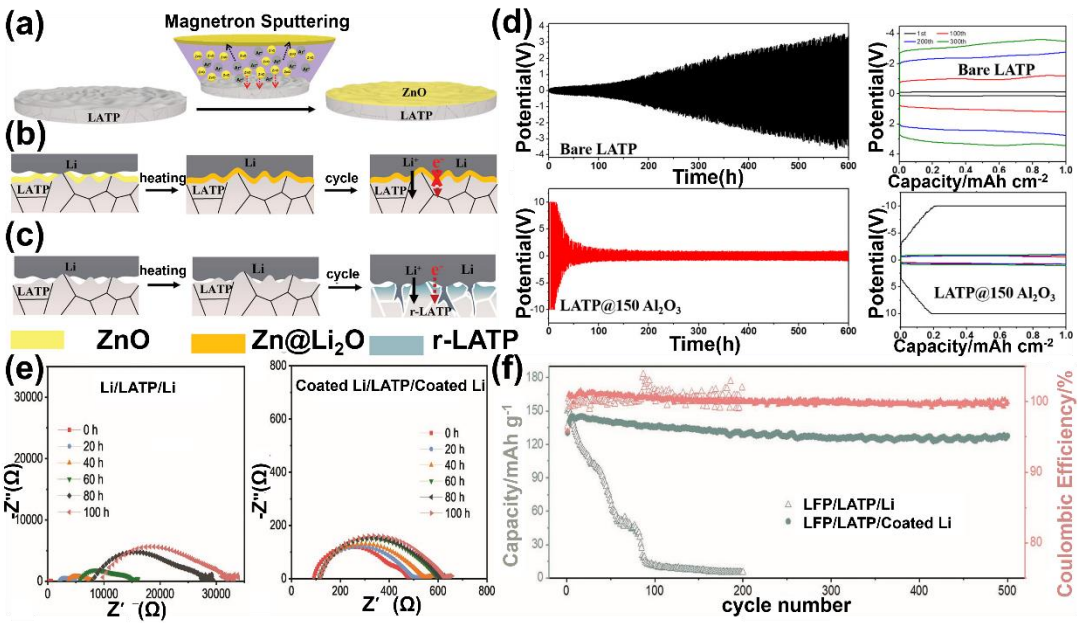

Figure 15. a) Schematic illustration of the preparation of LATP coated with a ZnO layer using magnetron sputtering, and the interface evolution between Li metal anode and LATP b) with and c) without the ZnO layer. Reproduced with permission.[178] Copyright 2019, Wiley-VCH. d) Electrochemical behavior, cycling behavior and voltage profile of the LATP/Li symmetrical cell with and without interlayer coatings at a current density of 0.01 mA cm^{-2}. Reproduced with permission.[35] Copyright 2018, American Chemical Society. e) EIS of LATP-Li symmetric cells without and with coated Li at 20 h intervals. Reproduced with permission.[179] Copyright 2020, Wiley-VCH. f) Long cycling performances and coulombic efficiencies of LFP/LATP/Li and LFP/LATP/coated Li SSB. Reproduced with permission.[179] Copyright 2020, Wiley-VCH.

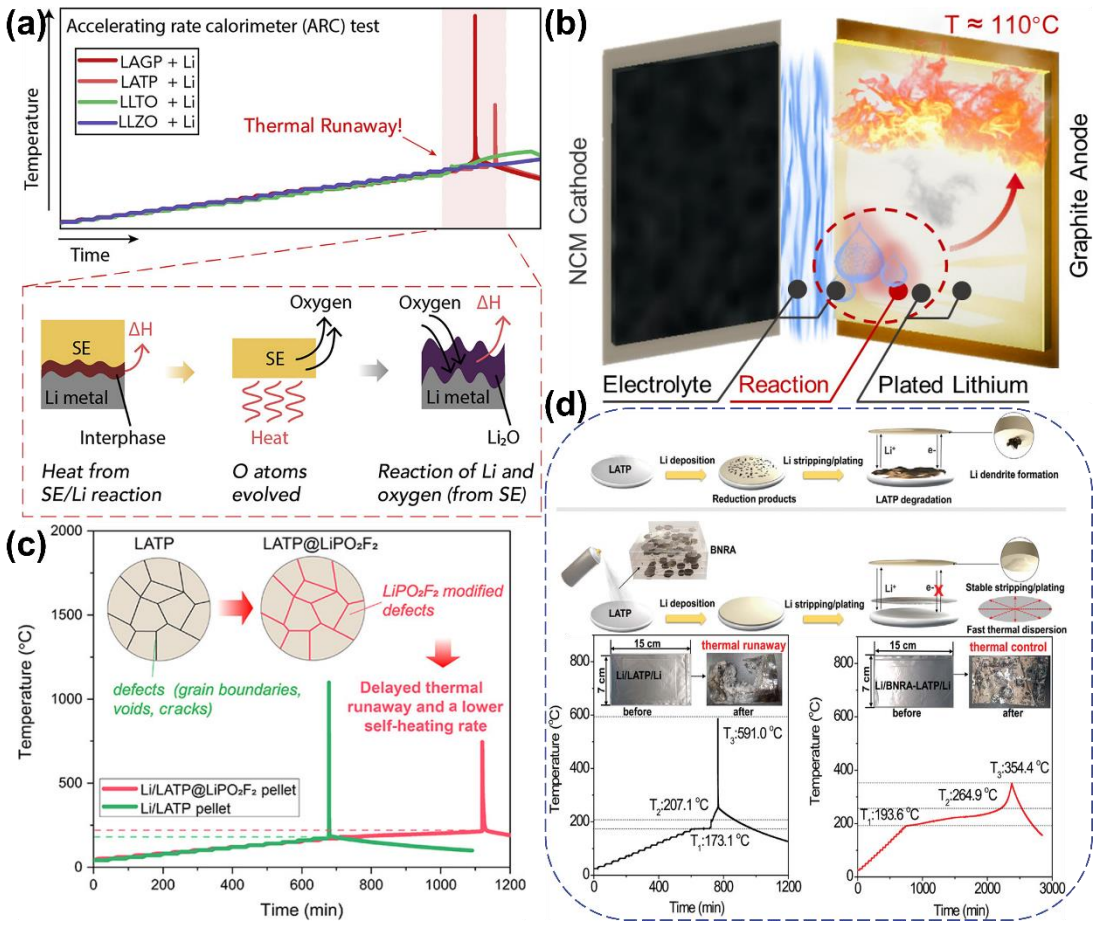

Figure 16. a) The thermal stability and heat runaway mechanism of Li-containing metal oxide SES. Reproduced with permission.[181] Copyright 2020, Elsevier. b) Schematic diagram of the thermal reaction of the battery after fast charging. Reproduced with permission.[180] Copyright 2019, American Chemical Society. c) The ARC test results of the Li/LATP pellet and the Li/LATP@$LiPO_2F_2$ pellet. Reproduced with permission.[168] Copyright 2021, American Chemical Society. d) Preparation and heat propagation experiments of LATP and BNRA-LATP samples. Reproduced with permission.[184] Copyright 2022, Wiley-VCH.

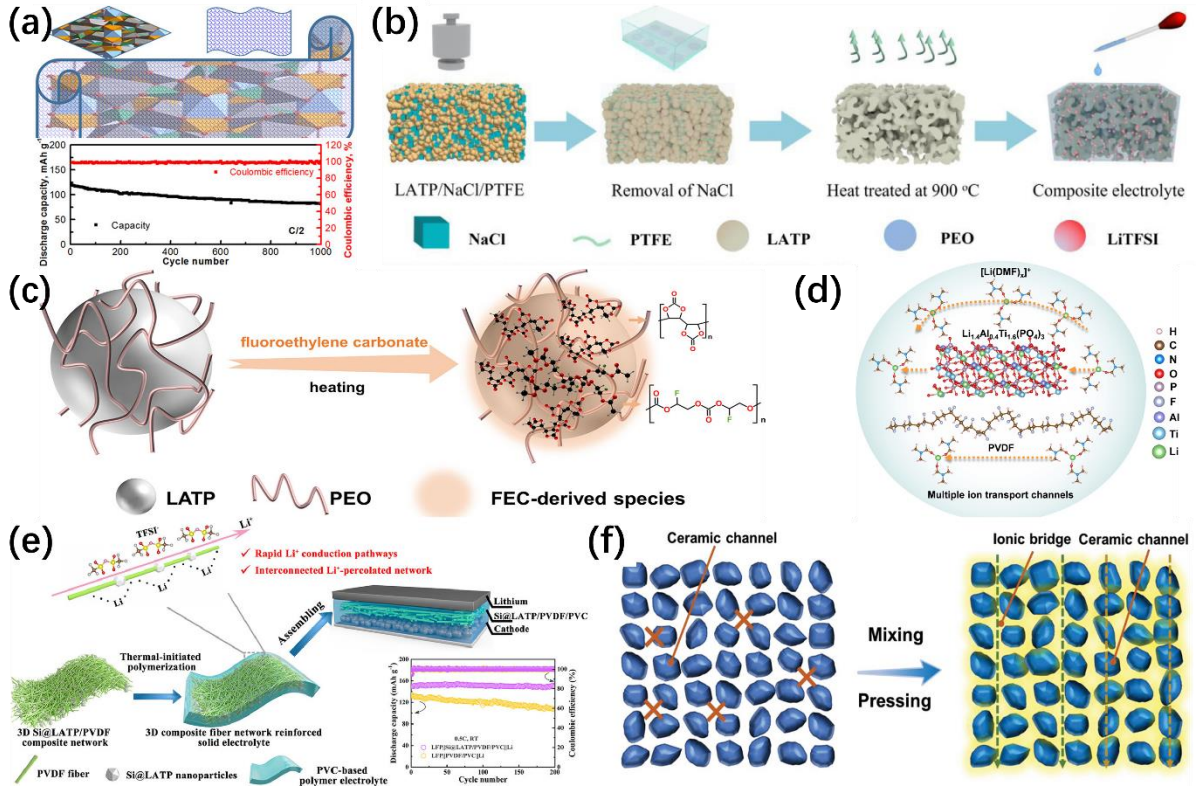

Figure 17. a) Schematic illustration of the slurry-casting method. Reproduced with permission.[193] Copyright 2020, American Chemical Society. b) Schematic illustration of the fabrication of CPE-3D. Reproduced with permission.[195] Copyright 2022, Elsevier. c) Schematic illustration of the fabrication of FEC@LATP. Reproduced with permission.[196] Copyright 2022, American Chemical Society. d) Li transport mechanism of composite electrolyte. Reproduced with permission.[200] Copyright 2021, Wiley-VCH. e) Schematic illustration of the fabrication of 3D Si@LATP/PVDF composite fiber network. Reproduced with permission.[203] Copyright 2022, Elsevier. f) Schematic illustration of the grinding and pressing method. Reproduced with permission.[209] Copyright 2021, Wiley-VCH.

Table 1 Summary of the basic properties of the typical solid-state electrolytes.

Classification	Material	Ionic conductivity [S cm^{-1}]	Activation energy [eV]	Ref.
Oxide	$Li_{1.3}Al_{0.3}Ti_{1.7}(PO_4)_3$	1.167×10^{-3} (RT)	0.22	[124]
	$Li_{1.5}Al_{0.5}Ge_{1.5}(PO_4)_3$	4×10^{-4} (RT)	0.37	[210]
	$Li_{0.34}La_{0.51}TiO_{2.94}$	1×10^{-3} (RT)	0.4	[211]
	$Li_7La_3Zr_2O_{12}$	2×10^{-6} (RT)	0.49	[212]
	$Li_{2+2x}Zn_{1-x}GeO_4$	3.9×10^{-7} (RT)	-	[213]
Solid Polymer Electrolytes	PEO−$LiClO_4$+ LATP	1.71×10^{-4} (RT)	0.03	[214]
	PEO−LiFSI	1.3×10^{-3} (80 °C)	-	[215]
Sulfide	$Li_{10}GeP_2S_{12}$	1.2×10^{-2} (RT)	0.25	[25]
	$0.7Li_2S-0.3P_2S$	1.7×10^{-2} (RT)	0.18	[216]
LiPON	LiPON	6.4×10^{-6} (RT)	0.47	[217]
	$Li_{3.3}PO_{3.9}N_{0.17}$	2×10^{-6} (RT)	~0.65	[218]

Table 2 Summary of synthesis methods, sintering temperature, purity and ionic conductivity of obtained $Li_{1+x}Al_xTi_{2-x}(PO_4)_3$ samples.

Synthesis method	*x*	Sintering temperature [°C]	Purity	Ionic conductivity [S cm^{-1}]	Ref.
Melt quenching	0.3	1000	$AlPO_4$ impurities	1.2×10^{-4} (RT)	[98]
	0.4	1000	$AlPO_4$ impurities	5.33×10^{-4} (RT)	[99]
Mechanical activation	0.3	775	$LiTiPO_5$ impurities	6.5×10^{-4} (RT)	[112]
	0.3	800	$Li_4P_2O_7$ impurities	3.1×10^{-4} (RT)	[111]
Sol–gel	0.3	950	Pure phase	3.44×10^{-4} (RT)	[110]
	0.3	800	Pure phase	8.5×10^{-4} (RT)	[117]
	0.3	900	Pure phase	1.2×10^{-4} (RT)	[86]
	0.3	900	$Li_4P_2O_7$ impurities	6×10^{-4} (30 °C)	[106]
	0.3	1000	Impurities	$\sim1\times10^{-3}$ (RT)	[100]
	0.3	1100	$AlPO_4$ impurities	4.2×10^{-4} (RT)	[118]
	0.4	950	Pure phase	5.9×10^{-4} (RT)	[116]
	0.5	850	Pure phase	6.9×10^{-4} (RT)	[113]
Co-precipitation	0.3	1000	$AlPO_4$ impurities	1.6×10^{-4} (RT)	[123]
	0.4	900	$AlPO_4$ impurities	1.83×10^{-4} (RT)	[122]
	0.5	825	$LiTiPO_5$ impurities	4.4×10^{-4} (RT)	[121]
	0.5	1000	Li_3PO_4 impurities	5.1×10^{-4} (30 °C)	[120]
Hydrothermal synthesis	0.3	890	Pure phase	3.15×10^{-4} (RT)	[128]
	0.3	900	$Li_4P_2O_7$ impurities	4.8×10^{-4} (30 °C)	[129]
	0.3	1075	Pure phase	1.167×10^{-3} (RT)	[124]
	0.3	1100	$LiTiPO_5$ impurities	2.7×10^{-4} (RT)	[127]
Spray-drying	0.3	900	$AlPO_4$ impurities	1.6×10^{-4} (30 °C)	[131]
	0.3	900	Pure phase	3.089×10^{-4} (RT)	[130]
Template method	0.3	950	$AlPO_4$ impurities	3.44×10^{-4} (RT)	[132]
Direct ink Writing	0.3	950	$LiTiPO_5$ impurities	4.24×10^{-4} (RT)	[133]
Pulsed laser deposition	0.3	1000	$AlPO_4$ impurities	1×10^{-4} (RT)	[134]

Table 3 Preparation method, sintering temperature, chemical formula and ionic conductivity of LATP with different ionic substitutions.

Method	Sintering temperature [℃]	Ionic substitution	Formula	Ionic conductivity [S cm^{-1}]	Ref.
Mechanical activation	1100	V replaces P	$Li_{1.3}Al_{0.3}Ti_{1.7}(PO_4)_{2.9}(VO_4)_{0.1}$	7×10^{-4} (RT)	[91]
Mechanical activation	850	Y replaces Al	$Li_{1.3}Al_{0.225}Y_{0.075}Ti_{1.7}(PO_4)_3$	8×10^{-4} (RT)	[143]
Co-precipitation	1000	Si replaces P	$Li_{1.7}Al_{0.3}Ti_{1.7}Si_{0.4}P_{2.6}O_{12}$	1.33×10^{-3} (RT)	[146]
Sol-gel	900	Cl replaces O	$Li_{1.3}Al_{0.3}Ti_{1.41}(PO_{3.61}Cl_{0.39})_3$	4.23×10^{-4} (RT)	[147]
Sol-gel	850	S replaces O	$Li_{1.3}Al_{0.3}Ti_{1.7}P_3O_{11.98}S_{0.02}$	5.21×10^{-4} (40 ℃)	[148]

Table 4 Additives, form, method and ionic conductivity of $Li_{1+x}Al_xTi_{2-x}(PO_4)_3$.

Additive	*x*	Method	Ionic conductivity [S cm^{-1}]	Ref.
15 wt% PEO 15 wt% BPEG	0.3	Mechanical activation	2.5×10^{-4} (60 °C)	[151]
8 wt% Nb_2O_5	0.5	Sol-gel	3.54×10^{-4} (30 °C)	[153]
10 wt% LBSO	0.3	Mechanical activation	1.5×10^{-4} (RT)	[74]
0.7 wt% SnO-P_2O_5-MgO	0.3	Mechanical activation	2.45×10^{-4} (RT)	[152]

Prof. Xin Su is the director of the Advanced Battery Technology Center, Harbin Institute of Technology, Weihai, with 15+ years of academic and industrial research and development (R&D) experience (from Brown University, Argonne National Lab, A123 systems LLC to Harbin Institute of Technology) in the field of battery materials and the design of lithium batteries. His current focus is materials and design of lithium batteries for various applications, including fundamental research, applied R&D, and manufacturing.

Prof. Brian W. Sheldon is a Professor of Engineering at Brown University. He holds an ScB in Chemical Engineering and an ScD in Materials Science, both from MIT. Prior to joining the Brown faculty, he was a research staff member at Oak Ridge National Laboratory. His research focuses on the formation and mechanical behavior of advanced ceramic materials, with signifi cant current efforts devoted to understanding degradation mechanisms in electrode materials for Li ion batteries.

 Dr. Wenquan Lu is the principal chemical engineer at Argonne National Laboratory with 20+ years experiences in the field of electrochemical energy storage area. Dr. Lu's current focus is lithium ion battery system development for electric vehicle (EV) applications, including fundamental understanding, applied R&D, and engineering. Having interest in R&D of advanced battery systems and other renewable energy (solar, wind etc.).